Lawrence Berkeley Laboratory
UNIVERSITY OF CALIFORNIA

Materials & Molecular Research Division

Presented at the NATO Advanced Study Institute, "Fundamental and Technological Aspects of Organo-F-Element Chemistry", Acquafredda di Maratea, Italy, September 10-21, 1984

ELECTRONIC STRUCTURE AND OPTICAL SPECTROSCOPY OF f^n IONS AND COMPOUNDS

N. Edelstein

October 1984

Prepared for the U.S. Department of Energy under Contract DE-AC03-76SF00098

DISCLAIMER

LBL-18582

ELECTRONIC STRUCTURE AND OPTICAL SPECTROSCOPY OF f^n IONS AND COMPOUNDS

Norman Edelstein
Materials and Molecular Research Division
Lawrence Berkeley Laboratory
University of California
Berkeley, California 94720 U.S.A.

ABSTRACT. The electronic structure of the actinides and lanthanides will be reviewed. The assignments of f^n spectra in the visible and near infra-red regions and the fitting of these spectra to the parameters of a phenomenological Hamiltonian will be discussed. From the wave-functions obtained from this type of analysis magnetic susceptibility data can be calculated. Examples will be given from recent work on $Cp_3Ln \cdot L$ ($Cp=C_5H_5$, L=base) compounds. Slater and spin-orbit parameters obtained from the analyses of free ion spectra and from the same ion in compounds will be compared.

1. INTRODUCTION

Optical spectra of f^n ions and compounds are characterized by relatively sharp lines due to transitions between energy levels within the f^n configuration. From analyses of these types of spectra, information may be obtained about the interactions between the f electrons of the ion and their surrounding ligands. The parametric theory used to obtain

this type of information is adapted from atomic theory and from the effects on the atom (or ion) of being placed in a crystalline environment. Essentially, this theory depends on the symmetry properties of the ion in the ligand field. In this review we will discuss how optical spectra of f^n ions in solids are analyzed, and calculate magnetic properties from the wavefunctions obtained from such an analysis. The $Cp_3Ln \cdot L$ ($Cp = \eta^5\text{-}C_5H_5$, L = base) complexes will be used as examples.

2. Review of Atomic Theory [1-4]

The quantum state of an atom is determined by the configuration which defines which one-electron eigenstates are occupied. The configuration is labelled by the quantum numbers n and ℓ where n is the principal quantum number and ℓ is the orbital quantum number. For example, Pr^{3+} has the following shells occupied: $1s^2$, $2s^2$, $2p^6$, $3s^2$, $3p^6$, $3d^{10}$, $4s^2$, $4p^6$, $4d^{10}$, $5s^2$, $5p^6$, $4f^2$, while for U^{4+}, the electronic configuration is: $1s^2$, $2s^2$, $2p^6$, $3s^2$, $3p^6$, $3d^{10}$, $4s^2$, $4p^6$, $4d^{10}$, $4f^{14}$, $5s^2$, $5p^6$, $5d^{10}$, $6s^2$, $6p^6$, $5f^2$. The closed shells of electrons contribute only a spherically averaged potential so we usually only consider the open shells and use the shorthand notation Pr^{3+} $[Xe]4f^2$; U^{4+} $[Rn]5f^2$.

The energy of the atom or ion is determined by the coupling of the open shell electrons. In our example of two equivalent f electrons we can have the orbital angular momentum of each electron adding together vectorally. Now $\ell = 3$ for an f electron so

$$\vec{L} = \sum_i \vec{\ell}_i = 6,5,4,3,2,1,0.$$

Each electron also has spin angular momentum so we have

$$\vec{S} = \sum_i \vec{s}_i = 1,0.$$

These two f electrons can form the following L-S terms: ^3S, ^1S, ^3P, ^1P, ^3D, ^1D, ^3F, ^1F, ^3G, ^1G, ^3H, ^1H, ^3I, ^1I. However the Pauli exclusion principle requires that two equivalent electrons cannot have the same quantum numbers. For example ^3I requires $s_1 = 1/2$, $s_2 = 1/2$, $\ell_1 = 3$, $\ell_2 = 3$ so this state is not allowed for two equivalent f electrons. By

similar arguments, the states ^3G, ^3D, and ^3S are also not permitted for equivalent electrons. If we construct a table showing the complete sets of electron configurations allowed for two equivalent f electrons classified by L_z and S_z where

$$L_z = \vec{\ell}_{zi} + \vec{\ell}_{zi} = \pm 6, \pm 5, \pm 4, \pm 3, \pm 2, \pm 1, 0$$

and

$$S_z = \vec{s}_{zi} + \vec{s}_{zi} = \pm 1, 0$$

we can show the allowed terms are

$$^1S,\ ^3P,\ ^1D,\ ^3F,\ ^1G,\ ^3H,\ ^1I.$$

These L-S terms differ in energy because of the Coulombic interaction between the two electrons, which is on the order of 10^3-10^5 cm^{-1}.

We now introduce magnetic interactions between the spin and the orbital angular momenta (spin-orbit coupling) which decompose the above L-S terms into individual levels of definite total angular momentum J where J is defined as

$$\vec{J} = \vec{L} + \vec{S}.$$

Schematically the energy level diagram for an f^2 configuration is shown in Figure 1. Note that each J level is (2J+1) degenerate and that this degeneracy may be lifted by an external electric field (i.e., a crystal field) and/or an external magnetic field.

For the f^2 configuration there are 13 J levels as shown in Figure 1. For higher values of n (in f^n) the number of J levels increases markedly. Table 1 shows the number of levels that can be obtained for various f^n configurations considering only the Coulombic and spin-orbit interactions [5].

Hund's rules, which determine the ground state of an atom for a particular configuration, are:

1. S is equal to its maximum value (consistent with the Pauli exclusion principle)
2. L is equal to its maximum value consistent with 1. (and the Pauli exclusion principle)
3. For a less than half-filled shell $J = J_{min} = L-S$.
   For a greater than half-filled shell $J = J_{max} = L+S$.

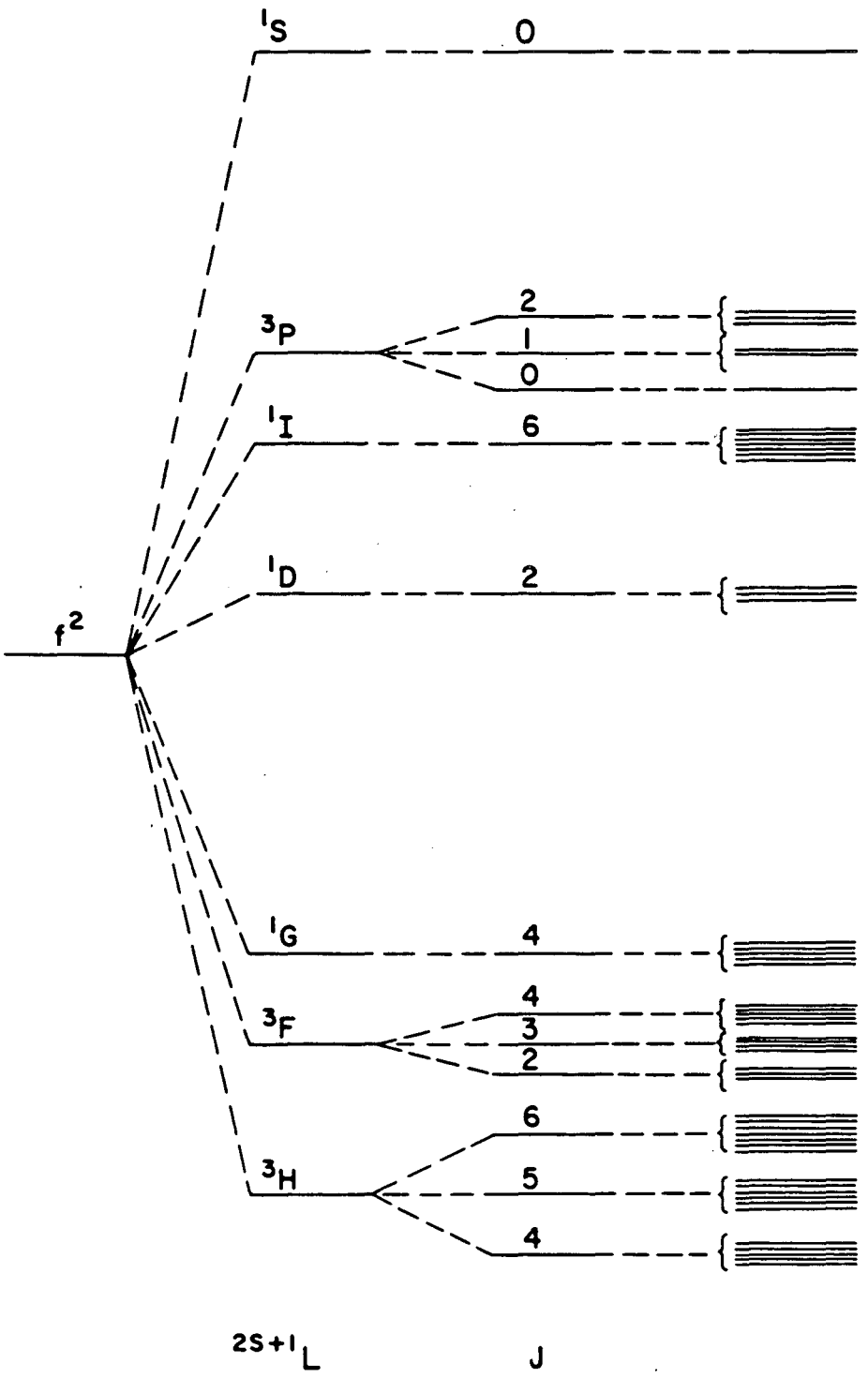

Figure 1. Schematic energy level diagram for the f^2 free ion.

Table 1. Number of levels considering various interactions for f^n configurations (From Ref. 5)

n =	1	2	3	4	5	6	7
H_1[a] (Maximum number of interacting levels)	1	1	2	4	7	9	10
Total number of multiplets	1	7	17	47	73	119	119
$H_1 + H_2$[b] (Maximum number of interacting levels)	1	3	7	19	30	46	50
Total number of J levels	2	13	41	107	198	295	327

[a] H_1 is the Coulombic interaction.

[b] H_2 is the spin-orbit interaction.

Applying these rules to the f^2 configuration we find the ground term is $^3H_4$.

The Coulombic and spin-orbit interactions represent the major interactions for equivalent electrons. However for highly accurate work we must also consider the effects of configuration interaction. This comes about by the mixing of other higher energy configurations into the ground configuration via the electrostatic repulsion term. For our example of f^2 this interaction could be with the excited 4f5d (5f6d) configuration or the 4f6s (5f7s) configuration. We will see later how these effects are treated with the parametric Hamiltonian.

Formally, for an N-electron atom with a nuclear charge Ze (e is the charge of the electron and Z is the atomic number), the non-relativistic

Hamiltonian is written (assuming the nuclear mass is infinite) as in eq. (1).

$$H = \sum_{i=1}^{N} \frac{p_i^2}{2m} - \sum_{i=1}^{N} \frac{Ze^2}{r_i} + \sum_{i<j}^{N} \frac{e^2}{r_{ij}} \qquad (1)$$

The first term in this equation represents the kinetic energy of all the electrons, the second term the potential energy of all the electrons in the electric field of the nucleus, and the third term the repulsive Coulomb potential between pairs of electrons.

In order to solve this equation we use the central field approximation for which the following assumptions are made:

1) Each electron is assumed to move independently.
2) There is a central field made up of the spherically averaged potential fields of each of the other electrons and the nucleus; that is, each electron is said to be moving in a spherically symmetric field (potential), $-\frac{U(r_i)}{e}$.

Then we may write the central field Hamiltonian as in eq. (2).

$$H_{CF} = \sum_{i=1}^{N} [\frac{p_i^2}{2m} + U(r_i)] \qquad (2)$$

This central field Hamiltonian results in a Schrodinger equation which may be readily solved in polar coordinates with wavefunctions of the form as shown in eq. (3).

$$\Psi = r^{-1} R_{n\ell}(r) Y_{\ell\ell_z}(\theta,\phi) \qquad (3)$$

These wavefunctions are products of the radial functions $R_{n\ell}(r)$ times the spherical harmonics $Y_{\ell\ell_z}(\theta,\phi)$, and the energy levels are highly degenerate. The energy levels are labeled by the principal quantum number n and the orbital quantum number ℓ. This degeneracy is removed by considering a number of perturbing effects.

For f electrons the most important perturbation is the term obtained by subtracting eq. 2 from eq. 1 (eq. (4)).

$$H - H_{CF} = \sum_{i=1}^{N} [-\frac{Ze^2}{r_i} - U(r_i)] + \sum_{i<j}^{N} \frac{e^2}{r_{ij}} . \qquad (4)$$

The first summation shifts all the levels in a given configuration equally so we will not consider it. The second term (eq. (5))

$$H_1 = \sum_{i<j}^{N} \frac{e^2}{r_{ij}} \tag{5}$$

represents the electrostatic Coulomb repulsion between pairs of electrons.

The energy levels of this electrostatic interaction are written in terms of the Slater integrals (eq. (6))

$$F^{(k)} = e^2 \int_0^\infty \frac{r_<^k}{r_>^{k+1}} [R_{nf}(r_i)R_{nf}(r_j)]^2 \, dr_i \, dr_j \tag{6}$$

where $r_<$ is the lesser and $r_>$ is the greater of r_i and r_j. The limitations on k are obtained from the properties of Legendre polynomials and are: k must be even, and $k \leq 2\ell$, which for f electrons means k is restricted to k = 0, 2, 4, 6. For example the electrostatic energy of the ^1I term is

$$E(^1I) = F^0 + \frac{F^2}{9} + \frac{F^4}{121} + \frac{25}{184041} F^6,$$

and the ^3H term is

$$E(^3H) = F^0 + \frac{F^2}{9} - \frac{17F^4}{373} - \frac{25F^6}{14157}$$

H_1 is diagonal in L and S which means we can label the eigenstates with particular eigenvalues of L and S in the form $^{(2S+1)}L$. This type of coupling is called Russell-Saunders coupling or L-S coupling.

To allow for relativistic corrections in the Hamiltonian we introduce H_2, the spin-orbit interaction as in eq. (7)

$$H_2 = \sum_i \xi(r_i) \, s_i \cdot \ell_i \tag{7}$$

or $H_2 = \zeta_{n\ell} S \cdot L$

where $\xi(r) = \frac{h^2}{2m^2c^2r} \frac{dU}{dr}$

and $\zeta_{n\ell} = \int_0^\infty R_{n\ell}^2 \xi(r) dr.$

The term H_2 becomes progressively more important as Z, the atomic number increases. This spin-orbit interaction is diagonal in J where $\vec{J} = \vec{L} + \vec{S}$. The interaction H_2 will couple ^{2S+1}L states whose value of S and L

differ by not more than one. The spin-orbit interaction is especially important for actinide ions because of their high values of Z. Then the L-S coupling scheme is no longer a valid approximation, and we speak of intermediate coupling.

The electrostatic and spin-orbit interactions represent the major effects in the parametric free-ion Hamiltonian. Nevertheless the combined diagonalization of these matrices and fitting of the F^k and ζ parameters sometimes results in calculated energy levels which are off by 100 cm^{-1} or more from the experimental values. These deviations result from the neglect of configuration interaction.

Configuration interaction arises from the interaction of excited configurations with the ground f^n configuration via the Coulombic field. Rajnak and Wybourne [3,6] have shown by second order perturbation theory that two-body effective operators

$$\alpha L(L+1) + \beta G(G_2) + \gamma G(R_7)$$

can be used to correct for these interactions. Here α, β, and γ are the two-body configuration interaction parameters, and $G(G_2)$ and $G(R_7)$ are Casimir's operators for the groups G_2 and R_7.

For f^n configurations with n = 3 or greater three body electrostatic configuration interaction parameters have been introduced by Judd [7,8]. These are written in the form

$$\sum_{k=2,3,4,6,7,8} T^k t_k$$

where T^k are the parameters and the t_k are the operators.

Effective operators [8] are used to parameterize small magnetic effects such as spin-spin and spin-other-orbit interactions and these are represented by the Marvin integrals M^0, M^2, and M^4 and written

$$\sum_{k=0,2,4} M^k m_k$$

with m_k as the operator. Finally the electrostatic-spin orbit interaction with higher configurations can be written as

$$\sum_{k=2,4,6} P^k p_k$$

with P^2, P^4, ,and P^6 as the parameters and the p_k as the operators.

In summary, the free ion parametric Hamiltonian is as shown in eq. (8).

$$H_{FI} = \sum_{k=0,2,4,6} f_k F^k(nf,nf) + \zeta_f a_{so} + \alpha L(L+1) + \beta G(G_2) + \gamma G(R_7) + \sum_{k=2,3,4,6,7,8} t_k T^k + \sum_{k=0,2,4} m_k M^k + \sum_{k=2,4,6} p_k P^k. \quad (8)$$

For an f^2 configuration, we have 14 parameters including F^0 while for an f^3 or higher configuration we have 20 parameters including F^0. The parameter F^0 just shifts the center of gravity of the configuration. Since we are only interested in the f^n configuration, it is set at a value such that the lowest level is equal to zero. In practice, ratios obtained from Hartree Fock calculations are sometimes used in the fitting procedures for the M^k and P^k parameters, or in cases of insufficient data, some parameters are set at the values obtained from Hartree-Fock calculations or extrapolated from other experimental data.

Now let us proceed with our f^2 example. Figure 2 shows the experimental levels for Pr^{3+}, $4f^2$ [9], and U^{4+}, $5f^2$ [10] while Table 2 gives the values found by fitting these levels with the parametric Hamiltonian [8,10].

Although the electrostatic interaction parameters are larger for Pr^{3+}, the spin-orbit coupling constant is much larger for U^{4+}. The net result is that the energy level diagrams for the two ions appear to be similar. This is partly due to the way in which the data are plotted; if we had started with the centers of gravity of the $4f^2$ and $5f^2$ configurations at zero energy, the relative strengths of the two interactions would have been more apparent. The eigenvectors listed on the figure clearly show the effects of the strong spin-orbit interaction in U^{4+}.

The energies of the identified levels of various configurations of the Pr^{3+} and U^{4+} free ions [9,11] are shown in Figure 3. In both cases the next higher configuration to the ground f^2 is the 4f5d (5f6d)

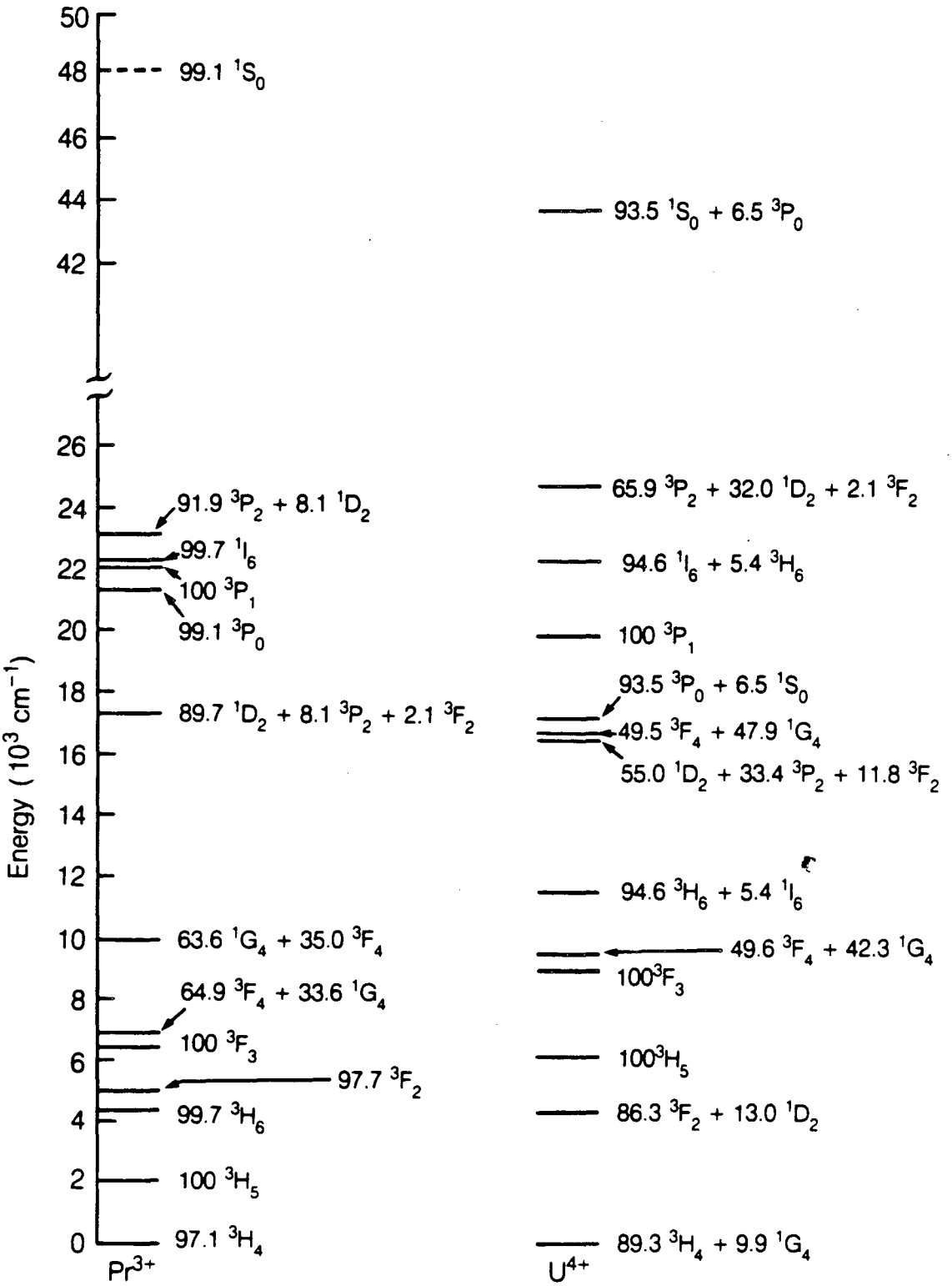

Figure 2. Experimental energy levels for Pr^{3+} and U^{4+} free ions (Refs. 9 and 10).

Table 2. Values of the Parameters for the Free Ions Pr^{3+} and U^{4+} (in cm^{-1})

	Pr^{3+} [a]	U^{4+} [b]
F^2	71822(35)	51938(39)
F^4	51827(93)	42708(100)
F^6	33890(60)	27748(68)
ζ_{nf}	766(2)	1968(2)
α	23.9(0.3)	35.5(.4)
β	-599(16)	-664(25)
γ	[1400]	744(26)
M^0	c	[.987]
M^2	c	[.550]
M^4	c	[.384]
P^2	166(38)	573(66)
P^4	c	524(144)
P^6	c	1173(321)
σ	- 11	9.8

[a] Ref. 8.

[b] Ref. 10.

[c] Values for these parameters are not given in Ref. 8.

configuration which starts at ~ 60,000 cm^{-1}. The higher configurations for the two ions are in approximately the same order, however at approximately 150,000 cm^{-1} there are some identified levels in U^{4+} from excitations from the closed shell, $6p^5 5f^3$. Analogous levels in Pr^{3+} have not been given.

Brewer [12] has tabulated the energies of the low-lying configurations of the free ions of the trivalent lanthanides and actinides. The energies of the lowest levels of various configurations with respect to the f^n configuration, as a function of atomic number,

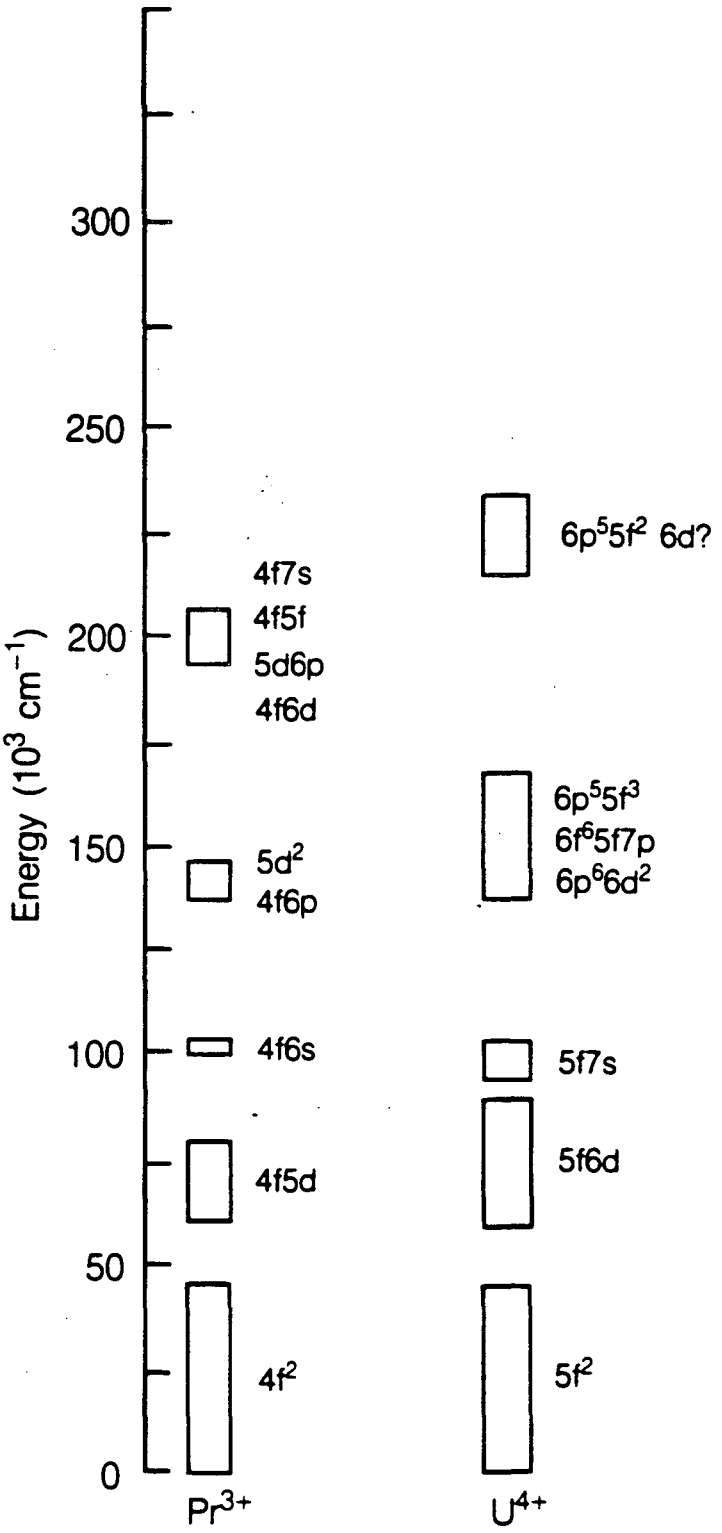

Figure 3. Assigned configurations for Pr^{3+} and U^{4+} free ions (Refs. 9 and 11).

are shown in Figure 4. Note that in general the curves for the actinide ions are somewhat lower than for the lanthanide ions. In particular the $5f^{n-1}6d$ configuration is below 50,000 cm^{-1} up through Pu^{3+}. In the solid state the 4f-5d transitions for RE^{3+} ions in CaF_2 are found to be ~18,000 cm^{-1} lower than for the free ions [13] as shown in Figure 5. If the same energy difference holds for the An^{3+} ions in the solid state, for U^{3+}-Pu^{3+} the 5f-6d transitions will be found below 30,000 cm^{-1}. For $U^{3+}/LaCl_3$ strong bands have been found at ~ 25,000 cm^{-1} which have been identified as f-d transitions [14].

The energy differences between the divalent rare earth free ions and the divalent ions in CaF_2 [15] are shown in Figure 6. In this case the ions, Ce^{2+}, Gd^{2+}, and Tb^{2+} in CaF_2 do not fit the systematic energy differences. In these ions, the $f^{n-1}d$ configuration may be the ground term or the $f^{n-1}d$ and f^n configurations may have their lowest crystal field states very close in energy. In either case,the assumption that the observed absorption bands are due to a transition from the lowest crystal field state of the f^n configuration to the lowest crystal field state of the $f^{n-1}d$ configuration would not be correct and would account for the deviations of these ions.

In the actinide series, Am^{2+}, Cf^{2+}, Es^{2+}, and all the elements with atomic number greater than 100 (except Lr) have well-characterized divalent states [16]. However, only sparse optical data exist. The energy differences between the trivalent and divalent free-ion states of the actinide series (for the same f^n configuration) are shown in Figure 7. In order to estimate the energies of the 5f-6d transitions for divalent and trivalent actinide ions in the solid state (for an f^n ground state), we assume the energy difference between the free ions and the ions in the solid state will be approximately the same as found for the lanthanide series. Assuming the energy differences of the $f^{n-1}d$ configurations are linear with oxidation state, Figure 7 can be used to estimate the energies of the $f^{n-1}d$ configuration for the tetravalent actinide free ions and for this oxidation state in compounds.

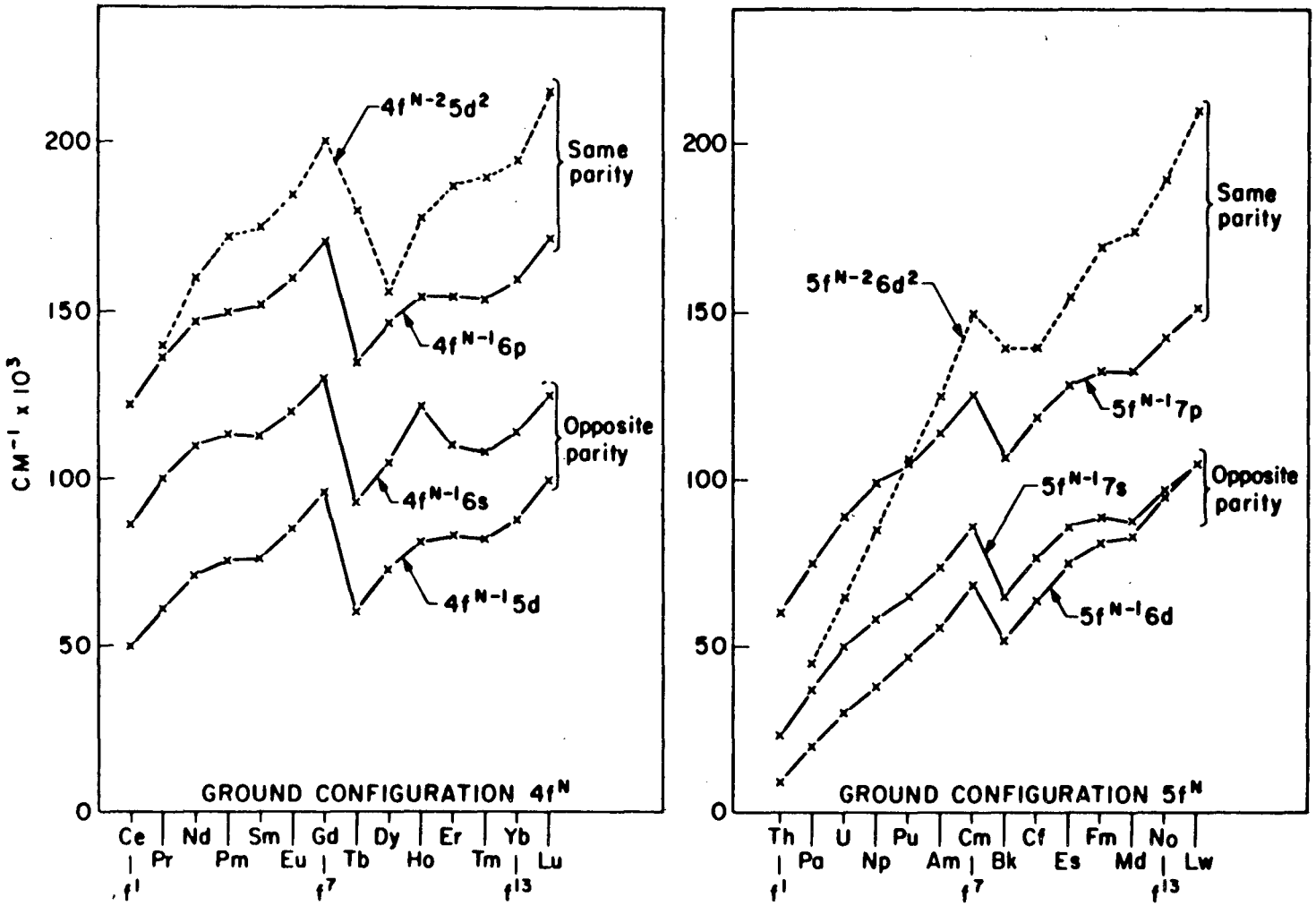

Figure 4. Energies of the lowest levels of various configurations of the trivalent lanthanides and actinides (Ref. 12).

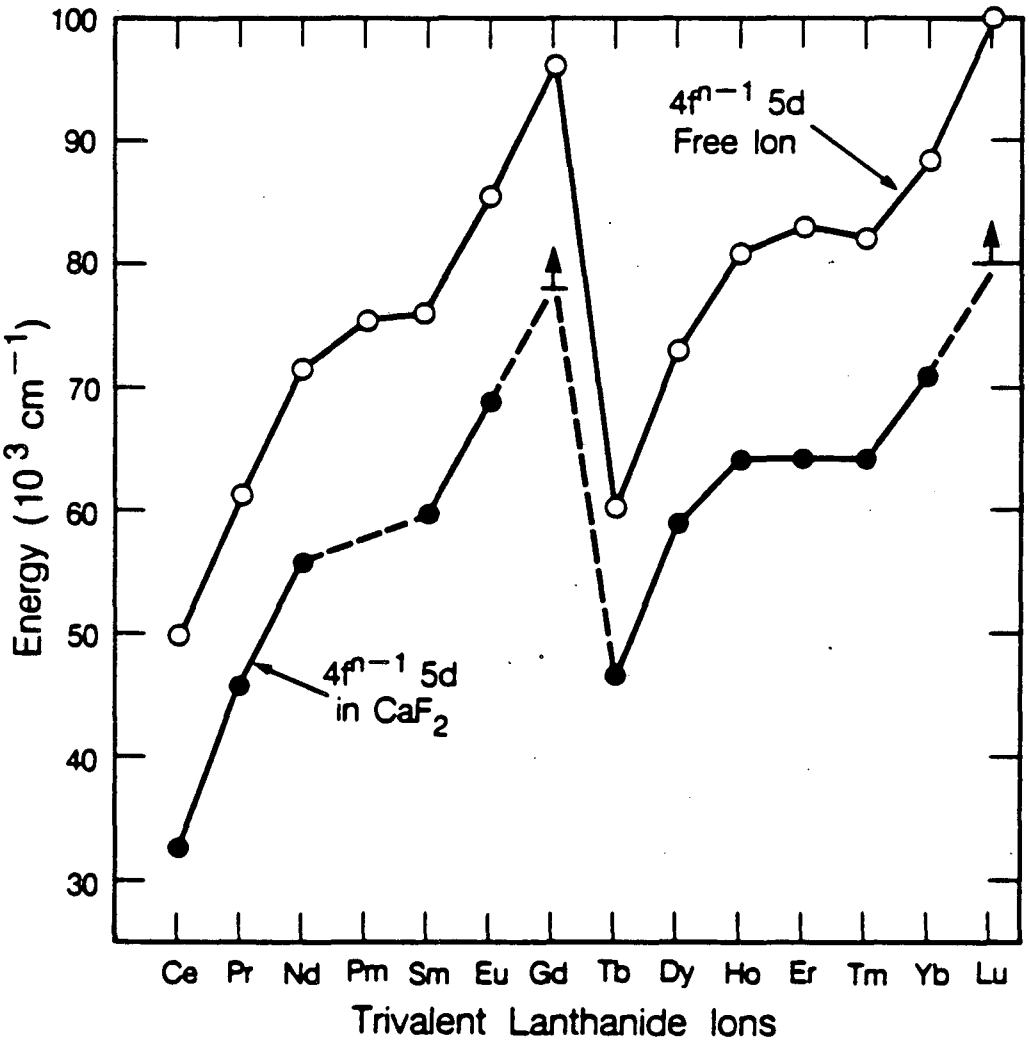

Figure 5. Energies of the lowest levels of the $4f^{n-1}$ 5d configuration for the trivalent lanthanide ions as free ions and in CaF_2 (Refs. 12 and 13).

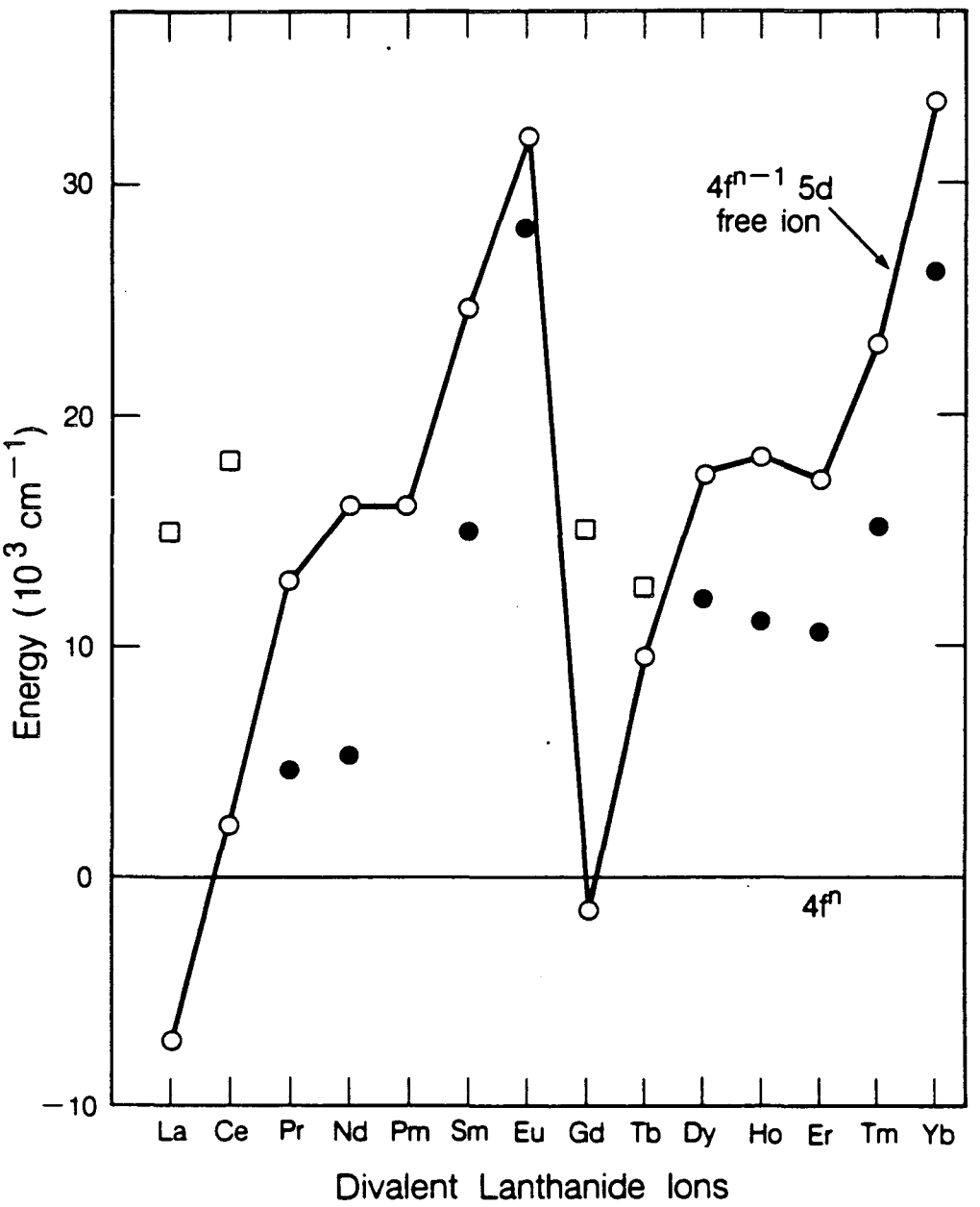

Figure 6. Energies of the lowest levels of the $4f^{n-1}$ 5d configuration for the divalent lanthanide ions as free ions (open circles) and in CaF_2 (filled circles and open squares) (Refs. 12 and 15).

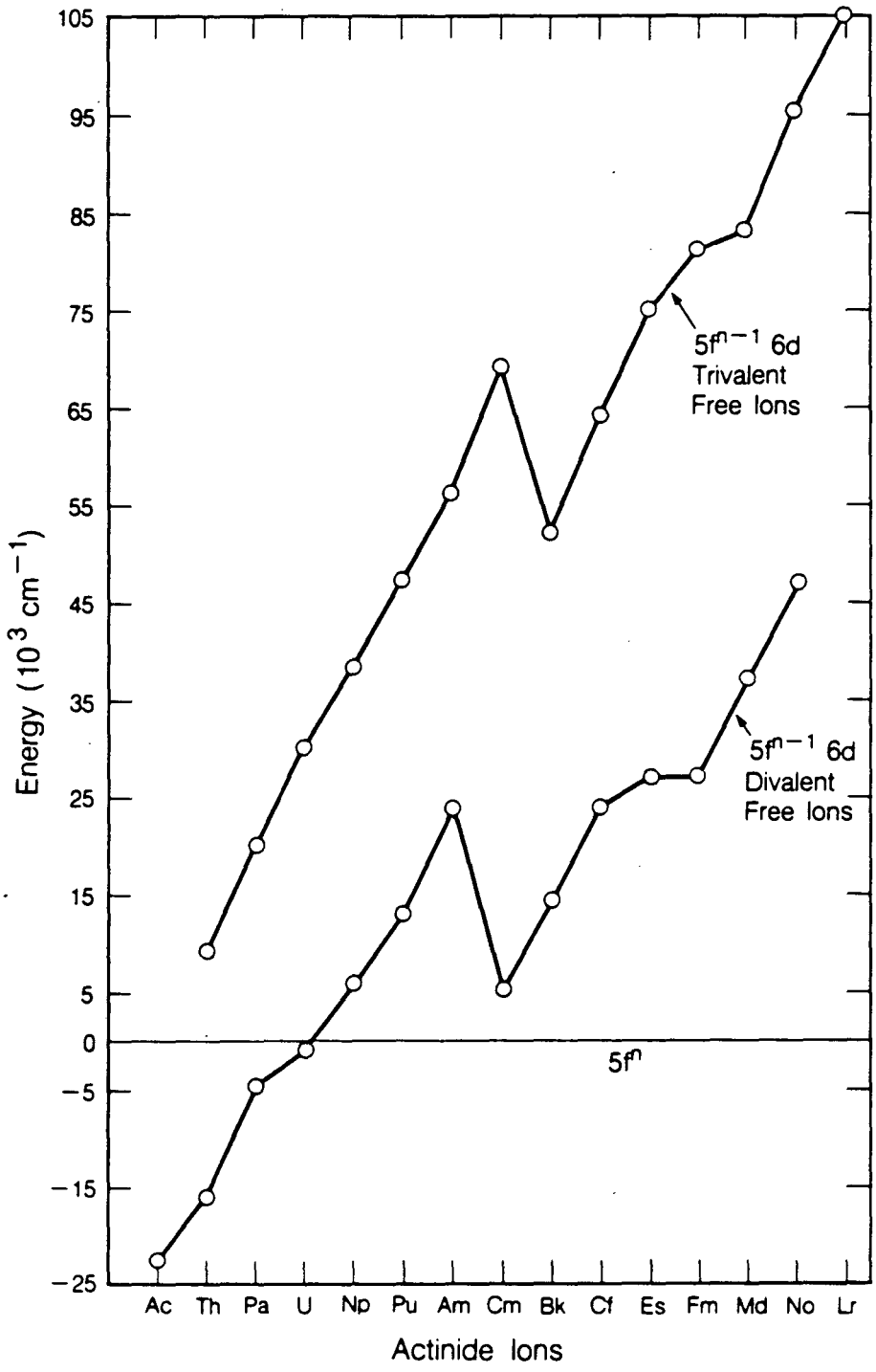

Figure 7. Energies of the $5f^{n-1}$ 6d configurations for the trivalent and divalent free ions of the actinide series (Ref. 12).

3. Crystal Fields

A free atom or an ion possesses spherical symmetry and each energy level is (2J+1)-fold degenerate. If this ion is placed in a crystal, each J level splits because of the electric field produced by this new environment. In crystals or compounds, the environment about the f^n ion possesses a well-defined symmetry (lower than spherical) and the splittings of the various J levels depends on the point symmetry of the site of the f^n ion. Table 3 shows the maximum number of states for various f^n ions and their LS terms [17]. For an ion with n (of f^n) odd, Kramers' theorem states that there remains a two fold degeneracy of the energy states which cannot be removed by the crystal field. This Kramers' degeneracy can be split by the application of a magnetic field.

We have previously discussed the free ion Hamiltonian. We now add a term to describe the potential at the f^n ion due to its surroundings (eq. (9)) [3]:

$$H_v = \sum_{k,q,i} B_q^k (C_q^k)_i, \quad [C_q^k = (\frac{4\pi}{2k+1})^{1/2} Y_q^k] \tag{9}$$

where the summation over i is over all open-shell electrons of the ion of interest. We can regard the B_q^k parameters as parameters to be determined experimentally, and the C_q^k are tensor operators whose matrix elements can be evaluated. The first term in the above expansion has k = q = 0 and is spherically symmetric. This term is by far the largest and is due to the Coulombic energy of a positive ion surrounded by negative charges, and corresponds to the lattice energy. For our purposes this term shifts all energy levels equally and does not contribute to the crystal field splittings. Since we are concerned only with equivalent f electrons, $k \leq 2\ell = 6$, and k has to be even. Therefore k = 2,4,6. The values of q are determined by the point symmetry of the f^n ion site, since the Hamiltonian must be invariant under the operations of the point symmetry group.

The general formula for the evaluation of crystal field matrix elements is given by [3,18] eq. (10).

Table 3. No. of LS states obtained from various f^n configurations (From Ref. 17). The italicized numbers refer to the number of times a term occurs, i.e. for $f^{4,10}$ $^1(S_2)$ means the ^1S term appears twice.

(1)	$f^{0,14}$	$^1(S)$			
(14)	$f^{1,13}$	$^2(F)$			
(91)	$f^{2,12}$	$^1(SDGI)$	$^3(PFH)$		
(364)	$f^{3,11}$	$^2(PD_2F_2G_2H_2IKL)$	$^4(SDFGI)$		
(1001)	$f^{4,10}$	$^1(S_2D_4FG_4H_2I_3KL_2N)$	$^3(P_3D_2F_4G_3H_4I_2K_2LM)$	$^5(SDFGI)$	
(2002)	$f^{5,9}$	$^2(P_4D_5F_7G_6H_7I_5K_5L_3M_2NO)$	$^4(SP_2D_3F_4G_4H_3I_3K_2LM)$	$^6(PFH)$	
(3003)	$f^{6,8}$	$^1(S_4PD_6F_4G_8H_4I_7K_3L_4M_2N_2Q)$	$^3(P_6D_5F_9G_7H_9I_6K_6L_3M_3NO)$	$^5SPD_3F_2G_3H_2I_2KL)$	$^7(F)$
(3432)	f^7	$^2(S_2P_5D_7F_{10}G_{10}H_9I_9K_7L_5M_4N_2OQ)$	$^4(S_2P_2D_6F_5G_7H_5I_5K_3L_3MN)$	$^6(PDFGHI)$	$^8(S)$

$$\langle f^n \alpha SLJJ_z | H_v | f^n \alpha' SL'J'J'_z \rangle \qquad (10)$$

$$= \sum B_q^k \langle f^n \alpha SLJJ_z | U_q^{(k)} | f^n \alpha SL'J'J'_z \rangle \langle f \| C^{(k)} \| f \rangle .$$

For f electrons

$$\langle f \| C^{(k)} \| f \rangle = \langle 3 \| C^{(k)} \| 3 \rangle = (-1)^3 [(7)(7)]^{1/2} \begin{pmatrix} 3 & k & 3 \\ 0 & 0 & 0 \end{pmatrix},$$

$$\langle f^n \alpha SLJJ_z | U_q^{(k)} | f^n \alpha' SL'J'J'_z \rangle$$

$$= (-1)^{J-J_z} \begin{pmatrix} J & k & J' \\ -J_z & q & J \end{pmatrix} \langle f^n \alpha SLJ \| U^{(k)} \| f^n \alpha' SL'J' \rangle$$

and

$$\langle f^n \alpha SLJ \| U^{(k)} \| f^n \alpha SL'J' \rangle$$

$$= (-1)^{S+L'+J+k} [(2J+1)(2J'+1)]^{1/2} \begin{Bmatrix} J & J' & k \\ L' & L & S \end{Bmatrix}$$

$$\times \langle f^n \alpha SL \| U^{(k)} \| f^n \alpha' S'L' \rangle .$$

Gathering all the terms

$$\langle f^n \alpha SLJUJ_z | H_v | f^n \alpha' SL'J'J'_z \rangle$$

$$= \sum B_q^{(k)} (-1)^{3-J_z+S+L'+2J+k} (7) \begin{pmatrix} 3 & k & 3 \\ 0 & 0 & 0 \end{pmatrix} \begin{pmatrix} J & k & J' \\ -J_z & q & J'_z \end{pmatrix} \begin{Bmatrix} J & J' & k \\ L' & L & S \end{Bmatrix}$$

$$\times [(2J+1)(2J'+1)]^{1/2} \langle f^n \alpha SL \| U^{(k)} \| f^n \alpha' SL \rangle .$$

In the above equation the () are 3-j symbols, {} is a 6-j symbol, and $\langle \| U^{(k)} \| \rangle$ is a reduced matrix element; the latter are tabulated for all f^n configurations by Nielson and Koster [19]. Note that S = S', if this is not true, the matrix element is zero. The above general equation for crystal field matrix elements may be readily evaluated by computer techniques.

Electric dipole transitions (f → f) are forbidden (to first order) by the Laporte selection rule which requires the transition matrix element to have even parity (the electric dipole operator has odd parity, therefore $\langle \psi_f | H_{ed} | \psi_f \rangle$ has odd parity). Van Vleck showed [20,21] the way out of this problem, pointing out that the f^n states can have

admixtures of higher configurations such as the $f^{n-1}d$ configuration which have the opposite parity. There are four types of transitions which can occur within an f^n configuration,

1. forced electric dipole transitions induced by odd components of the crystal field
2. forced electric dipole transitions induced by lattice vibrations
3. magnetic dipole transitions (allowed within an f^n configuration)
4. electric quadrupole transitions (allowed within an f^n configuration).

The last two types of transitions are usually orders of magnitude less intense than electric dipole transitions.

For crystals which are centrosymmetric, there are no odd components of the crystal field so transitions of type 1 cannot occur in this particular case. In fact for octahedral symmetry, the spectra are dominated by vibronic transitions, that is transitions which occur from the ground electronic and vibrational state to an excited electronic and vibrational state. In some cases, the 0-0 transition (from the ground state $v = 0$ to the excited state $v = 0$) is not observed and its energy is determined by assignment of the vibronic lines. For crystals without a center of symmetry the 0-0 lines are usually dominant. Magnetic dipole transitions are occasionally observed, but quadrupole induced transitions have not been assigned. Detailed selection rules are determined by the site symmetries of the ions in the crystals.

4. Examples of Crystal Field Analyses

The values of k and q allowed in the crystal field Hamiltonian are limited by the point group symmetry of the ion site and can be determined from the operations of the point symmetry group. Tabulations of the crystal field potential in various symmetries have been given [3,22]. Once the crystal Hamiltonian has been determined (i.e. the

values of k and q), it is convenient to introduce the crystal quantum numbers μ defined as

$$J_z = \mu \pmod{q}$$

where (mod q) means the addition or subtraction of multiples of q to the crystal quantum number μ.

D_{2d} symmetry is found in tetragonal crystals such as the orthophosphates and in $ThBr_4$. Our group has been analyzing optical data in these systems, and we will use them as examples [23-26]. The crystal field Hamiltonian in this symmetry is

$$H_{CF} = B_0^2 C_0^2 + B_0^4 C_0^4 + B_4^4 (C_4^4 + C_{-4}^4)$$

$$+ B_0^6 C_0^6 + B_4^6 (C_4^6 + C_{-4}^6).$$

Therefore k = 2,4,6, and q = 0,$\pm$4. We can classify the splittings of a particular J state in this crystal field according to the μ representation. This classification in D_{2d} symmetry is shown in Table 4 for all J states. For example a J = 6 state will be split into three non-degenerate μ = 0 states, three doubly degenerate $\mu = \pm 1$ states, and four non-degenerate μ = 2 states.

There are no crystal field matrix elements between states with different μ values. This scheme allows us to break up the energy matrix of the Hamiltonian into a set of smaller submatrices.

Another method that can be used to classify states is the use of the irreducible representations of the point symmetry groups. For configurations with an odd number of electrons, the crystal field levels belonging to non-cubic groups labeled by crystal quantum numbers and the irreducible representations of the point symmetry group have a one to one correspondence. However for an even number of electrons for C_{3v} or higher symmetries, some of the matrices obtained by the crystal quantum number scheme are reducible. In practice it is easier to construct the crystal quantum number matrices, and these matrices are diagonalized to obtain the energies. However, from the composition of the eigenvectors, the energy levels may be classified by the point group symmetry. It is useful to classify states by their irreducible representations because

Table 4. Crystal Quantum Numbers for D_{2d} Symmetry

Even Number of Electrons

μ	0	±1	2	No. of Levels
J	J_z	J_z	J_z	
0	0			1
1	0	±1		2
2	0	±1	2,2	4
3	0	3,±1,	2,2	5
4	-4,0,4	3,±1	2,2	7
5	-4,0,4	3,±1,±5	2,2	8
6	-4,0,4	3,±1,±5	-6,-2,2,6	10
7	-4,0,4	∓7,∓3,±1,±5	-6,-2,2,6	11
8	-8,-4,0,4,8	∓7,∓3,±1,±5	-6,-2,2,6	13
9	-8,-4,0,4,8	∓7,∓3,±1,±5,±9	-6,-2,2,6	14

Odd Number of Electrons

μ	±1/2	±3/2	±5/2	No. of Levels
J	J_z	J_z	J_z	
1/2	±1/2			1
3/2	±1/2	±3/2		2
5/2	±1/2	±3/2	±5/2	3
7/2	∓7/2,±1/2	±3/2	±5/2	4
9/2	∓7/2,±1/2	∓9/2,±3/2	±5/2	5
11/2	∓7/2,±1/2	∓9/2,±3/2	∓11/2,±5/2	6
13/2	∓7/2,±1/2,±13/2	∓9/2,±3/2	∓11/2,±5/2	7
15/2	∓7/2,±1/2,±13/2	∓9/2,±3/2,±15/2	∓11/2,±5/2	8

the selection rules for electric and magnetic dipole transitions can be easily worked out by the use of group theory.

Let us consider an even electron configuration, such as f^2, f^4,

f^{12}, etc. in D_{2d} symmetry. From the character table [27], we find five irreducible representations, four non-degenerate states Γ_1 - Γ_4, and one doubly degenerate state, Γ_5. To obtain the selection rules for electric and magnetic dipole radiation in D_{2d} symmetry, we note that z and x,y transform (transformation components of the electric dipole operator) as Γ_4 and Γ_5, respectively, and L_z and L_x, L_y (transformation components of the magnetic dipole operator) transform as Γ_2 and Γ_5. Now if we consider a matrix element of the type $\langle\psi_i|H_j|\psi_\ell\rangle$ where ψ_i, H_j, and ψ_ℓ transform according to the irreducible representations Γ_i, Γ_j, Γ_ℓ, this matrix element is zero unless $\Gamma_i \times \Gamma_j$ contains Γ_ℓ at least once. From the multiplication tables for D_{2d} symmetry we can easily work out the selection rules. These selection rules are shown in Table 5. The use of polarized radiation and application of these rules allow the assignment of various optical transitions to particular symmetry states for oriented single crystals. Verification of the assignments may be obtained by the calculation of the magnetic susceptibility of the compound and/or the measurement of the Zeeman splittings of the ground and excited states. It is the fact that single crystal samples are not readily available which has hampered the analysis of optical data of f element organometallics.

As an example of this type of analysis the Appendix presents a list of observed and calculated lines for Tm^{3+} ($4f^{12}$) diluted in a single crystal of $LuPO_4$ [26]. Most of this data was taken at 4.2^oK, and the assignments to the various symmetry states were made on the basis of linear polarization measurements. Data were also obtained at 77^oK where some higher lying crystal field states were populated. Since these higher states have a different symmetry than the ground level, transitions to different symmetry excited states are possible. Thus more levels may be assigned. Table 6 shows the parameters which have been obtained from this analysis.

Now Tm^{3+} is not much different in ionic radius than Lu^{3+}. We have measured the magnetic susceptibility of a pure crystal of $TmPO_4$ parallel and perpendicular to the crystallographic axis. Using the wave

Table 5A. Electric Dipole Transitions for D_{2d} Symmetry

	Γ_1	Γ_2	Γ_3	Γ_4	Γ_5
Γ_1				E_z[a]	$E_{x,y}$[b]
Γ_2			E_z		$E_{x,y}$
Γ_3		E_z			$E_{x,y}$
Γ_4	E_z				$E_{x,y}$
Γ_5	$E_{x,y}$	$E_{x,y}$	$E_{x,y}$	$E_{x,y}$	E_z

[a] E_z, the electric vector is parallel to the z axis (π_{el} spectrum).

[b] $E_{x,y}$, the electric vector is perpendicular to the z axis (σ_{el} spectrum).

Table 5B. Magnetic Dipole Transitions for D_{2d} Symmetry

	Γ_1	Γ_2	Γ_3	Γ_4	Γ_5
Γ_1		M_z[a]			$M_{x,y}$[b]
Γ_2	M_z				$M_{x,y}$
Γ_3				M_z	$M_{x,y}$
Γ_4			M_z		$M_{x,y}$
Γ_5	$M_{x,y}$	$M_{x,y}$	$M_{x,y}$	$M_{x,y}$	M_z

[a] Magnetic vector parallel to the z axis (or the electric vector perpendicular to the z axis) corresponding to σ_{mag}.

[b] Magnetic vector perpendicular to the z axis (or the electric vector parallel to the z axis) corresponding to π_{mag}.

Table 6. Parameters (cm^{-1}) obtained from the optical analysis of $Tm^{3+}/LuPO_4$ (From Ref. 26.)

Param.	Tm^{3+}
ζ	+2629.0(1)
F^2	101250(28)
F^4	70754(94)
F^6	50051(89)
B_0^2	203(22)
B_0^4	117(52)
B_4^4	-673(22)
B_0^6	-705(32)
B_4^6	16(33)
α	17.5(0.3)
β	-635(13)
γ	2200
M^0	4.93
M^2	2.72
M^4	1.37
P^2	729.6
P^4	547.0
P^6	364.0
σ	10.0

functions obtained from the optical analysis the parallel, perpendicular, and average magnetic susceptibilities have been calculated. The experimental and calculated susceptibilities are shown in Figure 8. As can be seen the agreement is very good.

The Cp_3Ln complexes and their adducts have been studied extensively by optical spectroscopy [28]. Much of the earlier work was done by Pappalardo [29-33], but recently Amberger and his coworkers [34-36] have started to reanalyze the old data and collect new data. Brittain et al. [37] have also reported luminescence data on $(RCp')_3Tb\cdot THF$ ($R=H,CH_3$; $Cp'=C_5H_4$). Pappalardo et al. have collected extensive line lists on a number of complexes using thin films and glasses, but the analyses have been hampered by the lack of single crystal data. In addition a number of the spectra are complicated by the presence of strong vibronic bands.

Amberger and coworkers have used the technique of magnetic circular dichroism (MCD) to obtain further information about the assignments of the states [34-36]. With this new data it has been possible to assign the optical spectra of $Cp_3Pr\cdot MeTHF$ and $Cp_3Pr\cdot CNC_6H_{11}$ [36]. By assuming the crystal field parameters obtained from the $Cp_3Pr\cdot L$ analyses can be used for the Nd complexes, the spectra of $Cp_3Nd\cdot MeTHF$ and $Cp_3Nd\cdot CNC_6H_{11}$ have been calculated and assigned [38]. This work will now be reviewed.

From structural studies on $Cp_3Pr\cdot CNC_6H_{11}$ and $Cp_3La\cdot THF$ the site symmetry about the trivalent ion is approximately C_{3v} [39,40]. The crystal field Hamiltonian in this symmetry is:

$$H_{CF} = B_0^2C_0^2 + B_0^4C_0^4 + B_3^4(C_{-3}^4 - C_3^4) + B_0^6C_0^6 + B_3^6(C_{-3}^6 - C_3^6) + B_6^6(C_{-6}^6 + C_6^6).$$

For an even number of electrons the states are classified as two non-degenerate states Γ_1 and Γ_2, and one doubly degenerate state Γ_3 [27]. The crystal quantum numbers for C_{3v} symmetry are shown in Table 7.

The MCD experiment measures the difference in absorption between right and left circularly polarized radiation in a magnetic field. This technique is useful because, in favorable cases, the line shape can be

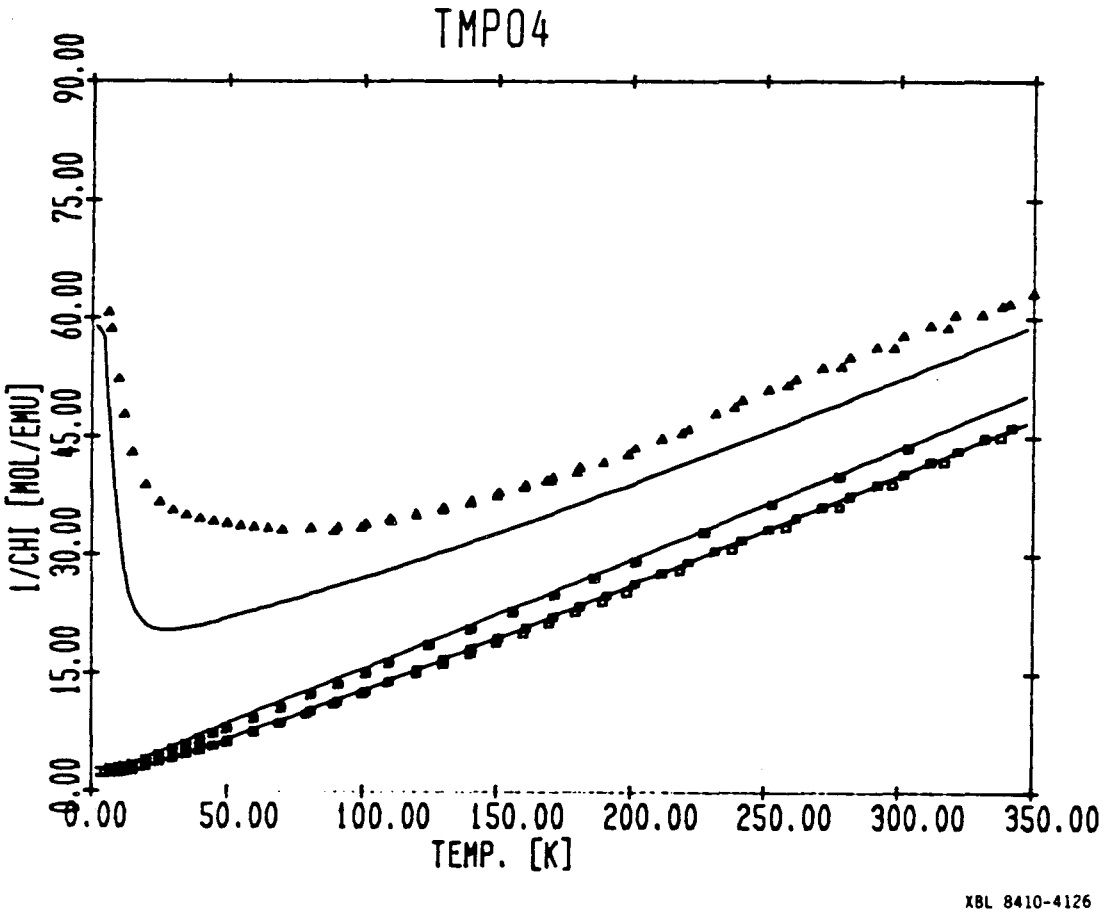

Figure 8. Plot of $1/\chi_M$ vs. T for $TmPO_4$; the continuous lines are calculated from the wavefunctions obtained from the optical spectrum, the points are experimental. The upper curve is for H∥z, the lower curve is for H⊥z, and the middle curve is for the powder.

used to determine the components of eigenvectors of the transitions under study [41,42]. The selection rules are given by

$$J'_z - J_z = \Delta J_z = -(\rho + q)$$

where $\rho = +1$ or -1 corresponding to right or left circularly polarized light. For C_{3v} symmetry $q = 0, \pm 3, \pm 6$. This technique gives the same information one could obtain from Zeeman measurements on oriented single crystals. The fact that it can be applied to solutions and randomly

Table 7. Crystal quantum numbers for C_{3v} symmetry

Even Number of Electrons			
μ	0	±1	No. of Levels
J	J_z	J_z	
0	0		1
1	0	±1	2
2	0	∓2,±1	3
3	-3,0,+3	∓2,±1	5
4	-3,0,+3	∓2,±1,±4	6
5	-3,0,+3	∓5,∓2,±1,±4	7
6	-6,-3,0,+3,+6	∓5,∓2,±1,±4	9
7	-6,-3,0,+3,+6	∓5,∓2,±1,±4,±7	10
8	-6,-3,0,+3,+6	∓8,∓5,∓2,±1,±4,±7	11
9	-9,-6,-3,0,+3,+6,-9	∓8,∓5,∓2,±1,±4,±7	13

Odd Number of Electrons			
μ	±1/2	±3/2	No. of Levels
J	J_z	J_z	
1/2	±1/2		1
3/2	±1/2	±3/2	2
5/2	5/2,±1/2	±3/2	3
7/2	5/2,±1/2,±7/2	±3/2	4
9/2	5/2,±1/2,±7/2	±3/2,±9/2	5
11/2	∓11,∓5/2,±1/2,±7/2	±3/2,±9/2	6
13/2	∓11,∓5/2,±1/2,±7/2,±13/2	±3/2,±9/2	7
15/2	∓11,∓5/2,±1/2,±7/2,±13/2	±3/2,±9/2,±15/2	8

ordered samples makes it especially valuable for organometallic compounds.

Magnetic susceptibility experiments show that $Cp_3Pr{\cdot}L$ compounds exhibit temperature independent paramagnetism [34] which means the ground state is a singlet. At low temperatures only the ground state should be appreciably populated, and MCD transitions which have derivative shaped lines (A terms) should correspond to transitions to the magnetic Γ_3 states. From the sign of the derivative curve (determined by whether the high or low energy side is above the baseline) the main J_z components of the eigenvector may be determined. Figures 9 and 10 show the absorption spectrum and the MCD spectrum of $Cp_3Pr{\cdot}MeTHF$ in the 510-540 nm region [35].

With the assignments obtained from the MCD spectra preliminary values of the crystal field parameters were obtained. These were then used to calculate the energy levels and further assignments were made on the basis of these calculations. Forty levels have been assigned with an rms deviation of 27.2 cm^{-1}. From the wavefunctions obtained from this analysis, the magnetic susceptibility was calculated. This is compared to the measured magnetic susceptibility of Cp_3Pr•butyl acetate (which has an optical spectrum very similar to that of Cp_3Pr•MeTHF) in Figure 11. A similar analysis has been carried out for $Cp_3Pr{\cdot}CNC_6H_{11}$. The empirical Hamiltonian parameters obtained from these analyses are given in Table 8 along with some other Pr^{3+} crystal and free ion data.

The Cp_3Pr•L crystal field parameters have been used to calculate the energy levels of Cp_3Nd•L compounds. As mentioned earlier, we assumed the crystal field parameters would not be much different for the Pr and Nd complexes. On this basis we were able to analyze the optical spectra

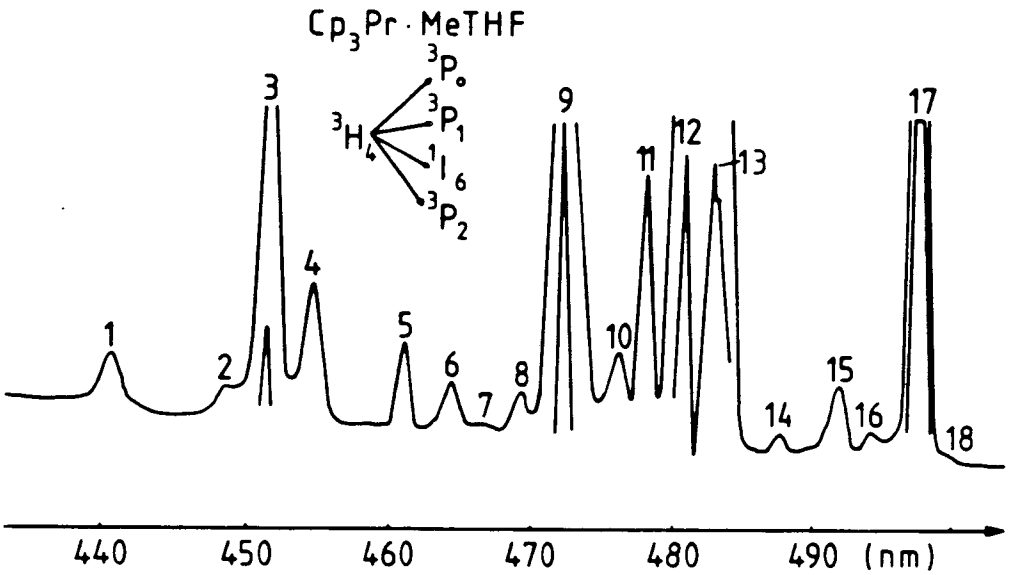

Figure 9. The absorption spectrum of Cp_3Pr•MeTHF in MeTHF in the region 510-430 nm at 10 K (Ref. 35).

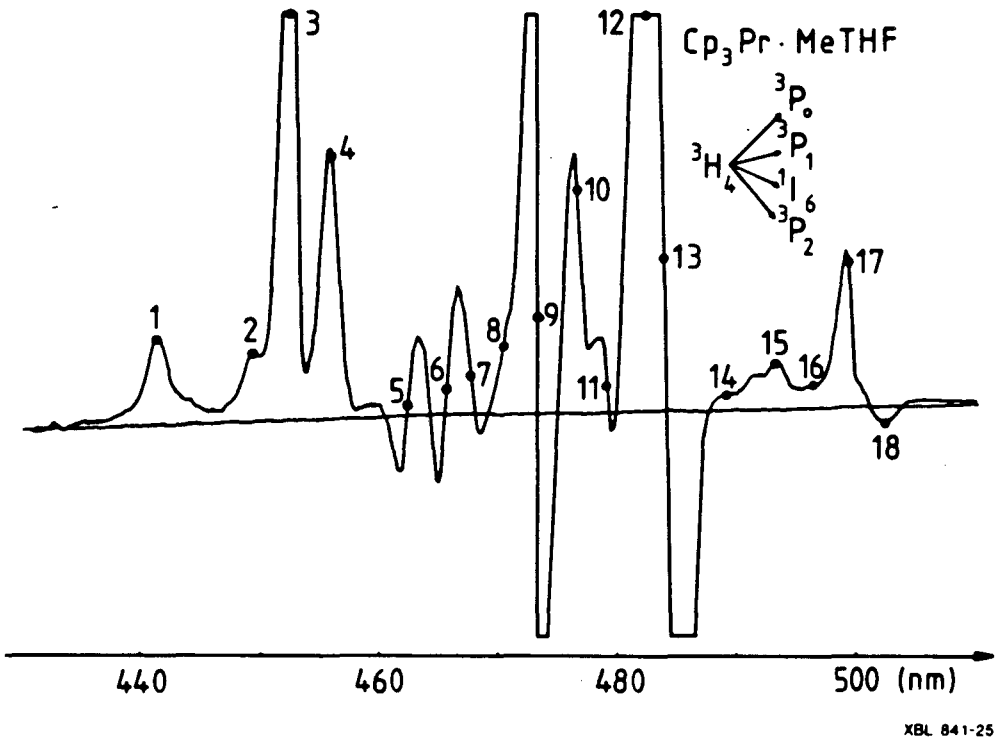

Figure 10. The MCD spectrum of $Cp_3Pr \cdot MeTHF$ in MeTHF in the region 510-401 nm at 30 K. The dots refer to maxima in the corresponding absorption spectrum (see Fig. 9) (Ref. 35).

of $Cp_3Nd \cdot MeTHF$ and $Cp_3Nd \cdot CNC_6H_{11}$ and assigned 70 levels with an rms deviation of 30.1 cm^{-1} for the MeTHF complex and 79 levels with an rms deviation of 26.8 cm^{-1} for the CNC_6H_{11} complex. The assignments for the $Cp_3Nd \cdot L$ complexes fit satisfactorily up to approximately 25000 cm^{-1}. At this energy a strong broad absorption band appears. Although f-f structure is superimposed on this band, the calculated assignments are off by 500-2000 cm^{-1}. Figures 12 and 13 show this region. The broad band is most likely a charge transfer transition and appears to interact in some fashion with the excited state f levels.

The empirical Hamiltonian parameters are given in Table 9. The calculated and experimental magnetic susceptibilities for $Cp_3Nd \cdot MeTHF$ are given in Figure 14.

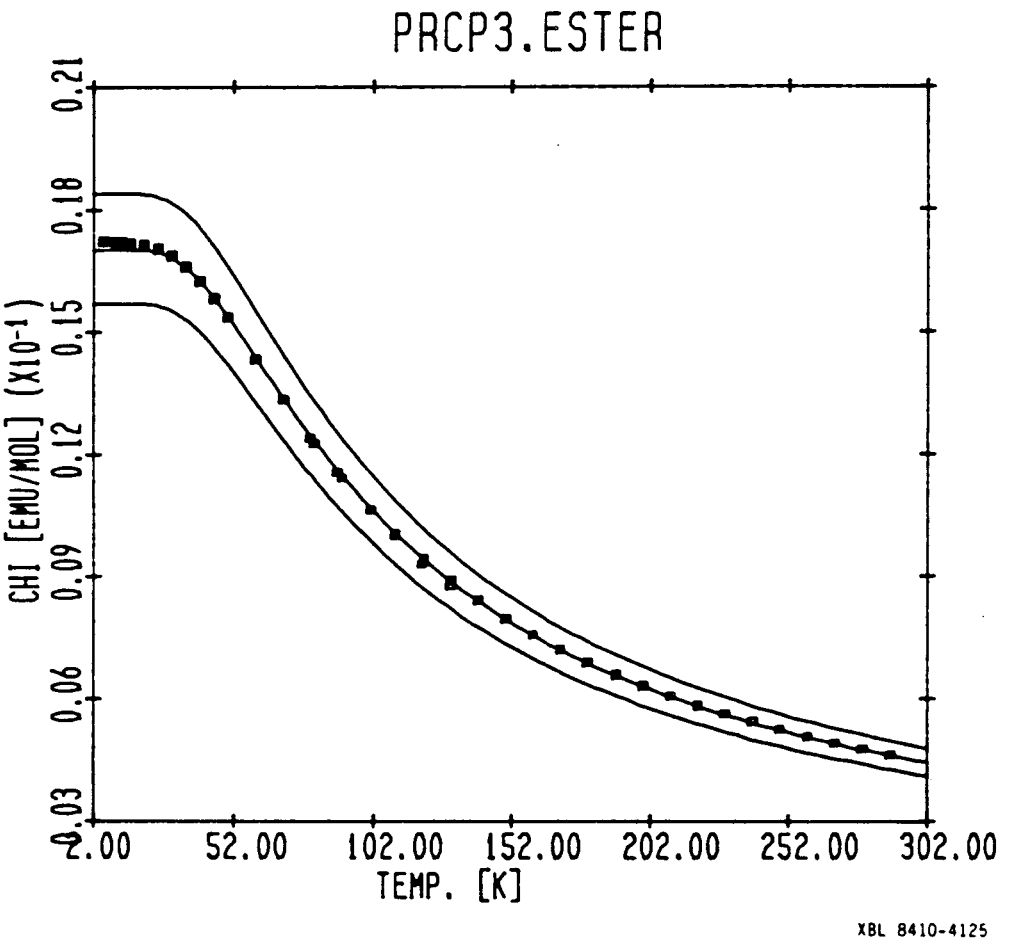

Figure 11. Calculated and experimental magnetic susceptibilities of $Cp_3Pr \cdot$butyl acetate as a function of temperature. The continuous lines are calculated for k=1.0, 0.975, and 0.95 from top to bottom where k is the orbital reduction factor; the squares are experimental points (Ref. 36).

Table 8. Parameter values for Pr^{3+} in various compounds (in cm^{-1}) (from Refs. 36 and 38)

Parameter	$Pr^{3+}/LaCl_3$ [a]	$Cp_3Pr \cdot MeTHF$	$Cp_3Pr \cdot CNC_6H_{11}$
F^2	68368	66207(62)	65607
F^4	50008	49184(178)	48120
F^6	32743	32543(126)	32170
ζ_{4f}	744	742(3)	735
α	22.9	23.1(0.5)	21.5
β	-674	-757(36)	702
γ	[1520] [b]	[1534]	[1534]
M^0	1.76 [e]	[1.76]	[1.76]
M^2	c	[0.99]	[0.99]
M^4	c	[0.67]	[0.67]
P^2	275	[275]	[275]
P^4	d	[206]	[205]
P^6	d	[138]	[138]
B_0^2	107	-1200(25)	-1361
B_0^4	-342	1301(76)	1580
B_0^6	-677	486(95)	786
B_3^4	-	290(68)	99
B_3^6	-	842(77)	918
B_6^6	466	-2035(59)	-2415
F^4/F^2	.73	.74	.73
F^6/F^2	.48	.49	.49
$\zeta_{cry}/\zeta_{free\ ion}$	.97	.97	.96

[a] From W.T. Carnall, H. Crosswhite, and H.M. Crosswhite, "Energy Level Structure and Transition Probabilities in the Spectra of the Trivalent Lanthanides in LaF_3," Argonne National Laboratory, 1977, unpublished.

[b] Values in [ ] held fixed in the fitting procedure.

[c] $M^2 = .56\ M^0$; $M^4 = .38\ M^0$

[d] $P^4 = .75\ P^2$; $P^6 = .50\ P^6$

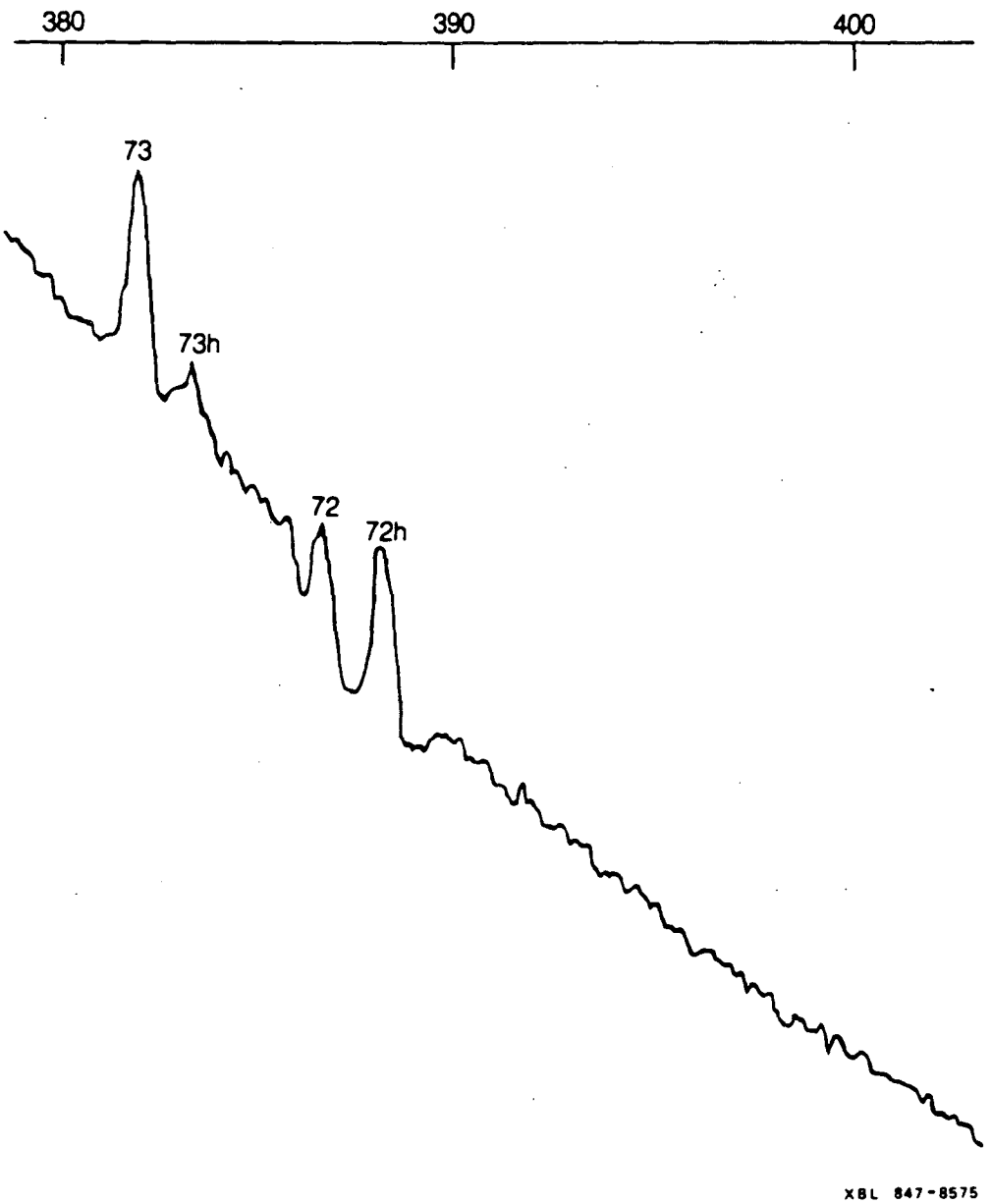

Figure 12. Absorption spectrum of $Cp_3Nd{\cdot}CNC_6H_{11}$ in glassy solution in the 380-440 nm region at -30 K (Ref. 38).

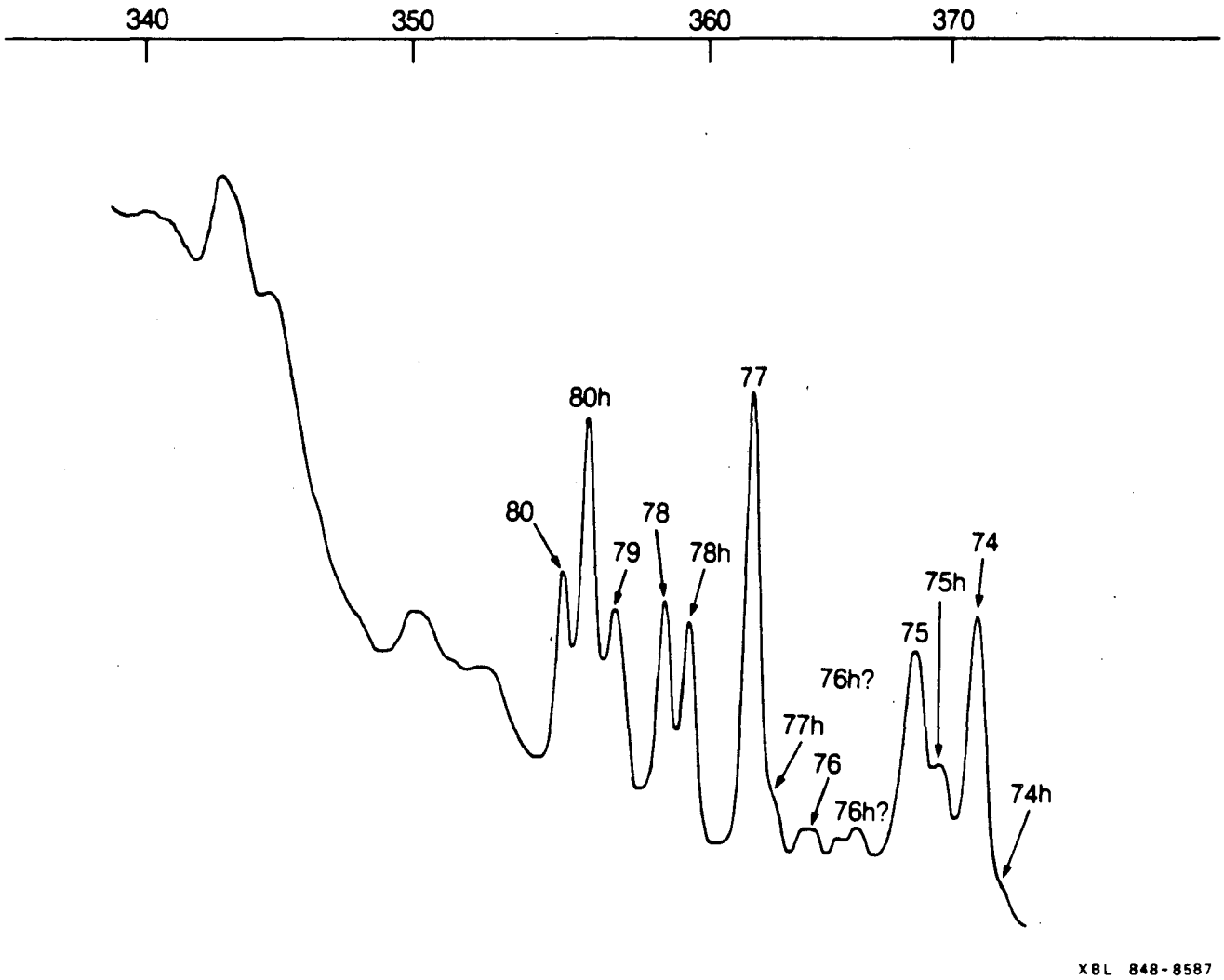

Figure 13. Absorption spectrum of $Cp_3Nd{\cdot}CNC_6H_{11}$ in glassy solution in the 340-380 nm region at ~30 K (Ref. 38).

Table 9. Parameter values for Nd^{3+} in various compounds (in cm^{-1})

	$Nd^{3+}/LaCl_3$ [a]	$Cp_3Nd \cdot MeTHF$ [b]	$Cp_3Nd \cdot CNC_6H_{11}$ [c]
F^2	71866(42)	70393(164)	70826(178)
F^4	52132(77)	51665(255)	51026(258)
F^6	35473(41)	35054(191)	35512(222)
ζ_{4f}	880(1)	882.3(2.5)	871.9(2.0)
α	22.08(0.10)	20.8(.6)	21.0(.5)
β	-650(5)	638(28)	642(24)
γ	1586(12)	[1586]	[1586]
T^2	377(15)	[377]	[377]
T^3	40(1)	[40]	[40]
T^4	63(3)	[63]	[63]
T^6	-292(5)	[-292]	[-292]
T^7	358(8)	[358]	[358]
T^8	354(11)	[354]	[354]
M^0	1.97(0.10)	[1.97]	[1.97]
M^2	[1.10]	[1.10]	[1.10]
M^4	[0.75]	[0.75]	[0.75]
P^2	255(23)	[255]	[255]
P^4	[192]	[191]	[191]
P^6	[128]	[127]	[127]
B_0^2	163(8)	-1838(50)	-1831(41)
B_0^4	-336(22)	1521(83)	1551(76)
B_0^6	-713(22)	279(138)	-74(117)
B_3^4	-	321(94)	626(81)
B_3^6	-	1128(70)	1246(65)
B_6^6	462(17)	-1271(94)	-1381(78)

---

[a] From H.M. Crosswhite, H. Crosswhite, F.W. Kaseta, and R. Sarup, J. Chem. Phys. 64, 1981 (1976). 101 levels fit; $\sigma = 8.1\ cm^{-1}$.

[b] 70 levels fit; $\sigma = 30.1\ cm^{-1}$ (Ref. 38).

[c] 79 levels fit; $\sigma = 26.8\ cm^{-1}$ (Ref. 38).

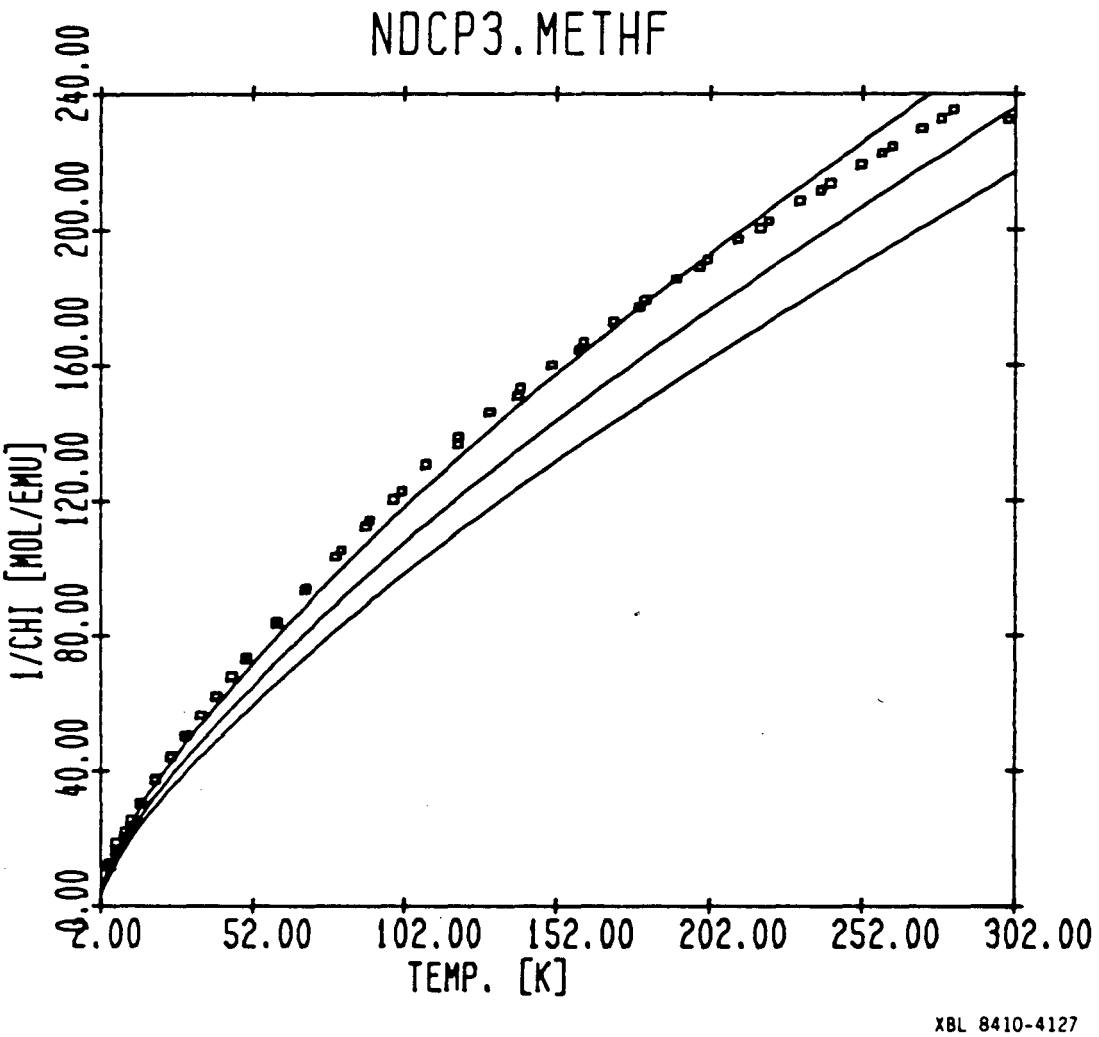

Figure 14. Plot of $1/\chi_M$ vs T for $Cp_3Nd \cdot MeTHF$ powder. The continuous lines are for k=0.95, 0.975, and 1.00 from top to bottom where k is the orbital reduction factor; the squares are experimental points.

5. DISCUSSION

The results of the recent optical analyses of $Cp_3Pr \cdot L$ and $Cp_3Nd \cdot L$ have been given. One of the most interesting aspects of this study is the large crystal field in these complexes. Auzel and Malta [43] have defined the parameter

$$N_v/(4\pi)^{1/2} = [\sum_{k,q} \frac{1}{2k+1} (B_q^k)^2]^{1/2}$$

as a measure of the relative strengths of the crystal field of ions in various symmetries. Table 10 lists this parameter for a number of ions in various crystals and compounds. Using the $N_v/(4\pi)^{1/2}$ parameter, the crystal fields for $Cp_3Ln \cdot MeTHF$ or $Cp_3Ln \cdot CNC_6H_{11}$ (Ln = Pr,Nd) are approximately three times greater than for Pr^{3+} and Nd^{3+} in $LaCl_3$.

Table 10. Comparison of the crystal field splittings for various systems.

Compound	$N_v/(4\pi)^{1/2}$ (cm^{-1})
$Pr^{3+}/LaCl_3$	259
$Nd^{3+}/LaCl_3$	271
$Ho^{3+}/LaCl_3$	200
$Pr^{3+}/LuPO_4$	547
$Nd^{3+}/LuPO_4$	478
$Tm^{3+}/LuPO_4$	314
$Cp_3Pr \cdot MeTHF$	936
$Cp_3Pr \cdot CNC_6H_{11}$	1100
$Cp_3Nd \cdot MeTHF$	1082
$Cp_3Nd \cdot CNC_6H_{11}$	1117
$U^{3+}/LaCl_3$	534
$Pu^{3+}/LaCl_3$	584
$U^{4+}/ThBr_4$	1340
$U(BD_4)_4$	3297

The values of the Slater parameters and the spin-orbit coupling constant for transition metal ions in crystals and molecules are smaller than the values found in the free ion. The extent of this reduction has been used as a measure of the covalency of the complex [44]. Newman has

suggested that the reduction in the values of the Slater parameters should be correlated with the ligand polarizability [45], but calculations by other workers have shown (for d transition metal ions and U^{4+}) [46,25] that this mechanism does not account for the large reductions found empirically. Some values of various ratios for Pr^{3+} and U^{4+} ($4f^2$ and $5f^2$) are shown in Table 11.

Table 11. Ratios of parameters for various systems.

Compound	$\frac{F^2_{cry}}{F^2_{FI}}$	$\frac{F^4_{cry}}{F^4_{FI}}$	$\frac{F^6_{cry}}{F^6_{FI}}$	$\frac{\zeta_{cry}}{\zeta_{FI}}$	$\frac{F^4_{cry}}{F^2_{cry}}$	$\frac{F^4_{FI}}{F^2_{FI}}$
$Pr^{3+}/LaCl_3$	.95	.96	.97	.97	.73	.72
$Pr^{3+}/LuPO_4$	.94	.94	95	.97	.72	.72
$Cp_3Pr\cdot MeTHF$	.92	.95	.96	.97	.74	.72
$Cp_3Pr\cdot CNC_3H_{11}$	.91	.93	.95	.96	.73	.72
$Nd^{3+}/LaCl_3$	-	-	-	-	.73	-
$Cp_3Nd\cdot MeTHF$	-	-	-	-	.73	-
$Cp_3Nd\cdot CNC_6H_{11}$	-	-	-	-	.72	-
$U^{3+}/LaCl_3$	-	-	-	-	-	.84
$Pu^{3+}/LaCl_3$	-	-	-	-	.81	
$U^{4+}/ThBr_4$	.81	.95	.93	.91	.96	.82
$U(BD_4)_4/Hf(BD_4)_4$	.79	.94	.81	.91	.97	.82
$Np(BD_4)_4/Zr(BD_4)_4$	.85[a]			.93[a]	.93	-

[a]Based on the predicted free ion values (see Ref. 47).

From Table 11 one can immediately note the similarity between the ratios for $Pr^{3+}/LaCl_3$ and $Cp_3Pr\cdot MeTHF$ and the differences with the ratios for $U^{4+}/ThBr_4$ and $U(BD_4)_4$. Clearly F^2 is much more affected by the crystalline environment than F^4 and F^6 so that in cases where free ion data is not available the ratio F^4/F^2 could be used to compare the same ion in different environments [47]. The reduction found for the spin-orbit coupling constant in $Cp_3Pr\cdot MeTHF$ agrees very well with the value of the orbital reduction constant ($k = 0.975$) found from the magnetic measurements. Thus, even though the crystal field is ~ 3 times larger in $Cp_3Pr\cdot MeTHF$ than in $Pr^{3+}/LaCl_3$, the reduction in F^2 and ζ is the same for these two compounds. A similar orbital reduction factor ($k = 0.95$) was needed in order to fit the $Cp_3Nd\cdot MeTHF$ magnetic data.

For the U^{4+} systems, $U^{4+}/ThBr_4$ and $U(BD_4)_4/Hf(BD_4)_4$, the ratios of F^2_{cry}/F^2_{FI} ~ 0.80. This reduction implies that tetravalent uranium compounds are quite covalent. In fact the reduction in the free-ion parameter F^2 is of the same order as found for Cr^{3+} ($3d^3$) in emerald or K_2NaCrF_6 or Co^{2+} ($3d^7$) in $CoCl_2$ [25,48].

Magnetic data are not available for $U(BD_4)_4$ in T_d symmetry. Figure 15 shows the magnetic susceptibility data for $U(BH_3CH_3)_4$ which has an optical spectcrum very similar to that of $U(BD_4)_4/Hf(BD_4)_4$ [48]. Curve C of Fig. 15 is calculated from the parameters of the optical fit. From the optical analysis $\zeta_{cry}/\zeta_{FI} = 0.91$. If we use this value for the orbital reduction constant, curve D is obtained. In order to get curve E the splitting between the ground E state and the first excited T_1 state was adjusted to 215 cm^{-1} and k was set equal to 0.85 [48]. This value of the orbital reduction constant confirms a greater covalent interaction for $U^{4+}/ThBr_4$ or $U(BD_4)_4$ than in the $Cp_3Pr\cdot L$ compounds.

The analysis of the optical spectrum of $Np(BD_4)_4/Zr(BD_4)_4$ and the electron paramagnetic resonance of $Np(BD_4)_4$ and $Np(BH_3CH_3)_4$ have recently been presented [47]. Some of the ratios obtained from the optical analysis are given in Table 11. Using the predicted value of 2253 cm^{-1} for ζ_{FI} of Np^{4+}, $\zeta_{cry}/\zeta_{FI} = 0.93$ for $Np(BD_4)_4$ which represents a slight increase as compared to $U(BD_4)_4$. The predicted value of F^2 for

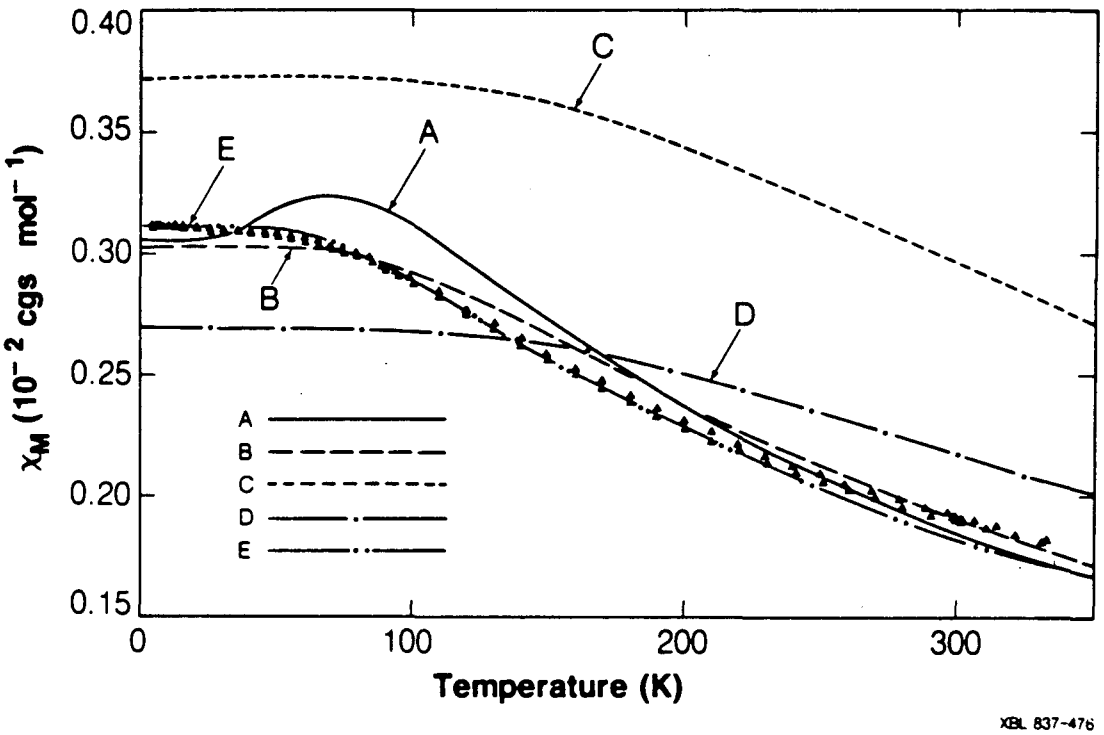

Figure 15. Plot of χ_M vs. T for $U(BH_3CH_3)_4$. Lines A and B are calculated by considering only the $^3H_4$ multiplet; however the crystal field parameters are quite different than those obtained from the optical analysis. Line C is calculated from the parameters of optical analysis; line D is the same as C with k=0.91. Line E is the same as C but with the $T_1(^3H_4)$ moved to 215 cm^{-1} and k=0.85 (Ref. 48).

the Np^{4+} free ion leads to $F^2_{FI}/F^2_{cry} = 0.86$ vs. 0.81 for U^{4+}. From Crosswhite et al. [14] we obtain values of F^4_{cry}/F^2_{cry} for the trivalent actinides in $LaCl_3$. The results shown in Table 11 indicate a decrease in this ratio on going from U^{3+} to Pu^{3+}. These numbers are all consistent with increasing covalency with increasing oxidation number and decreasing covalency with increasing Z, the atomic number, for both the trivalent and tetravalent actinides. These results can be

rationalized by considering the actinide contraction and increased screening of the 5f electrons as Z increases.

From the epr data for $Np(BH_4)_4$ and $Np(BD_4)_4$ shown in Table 12 we see that the wave function obtained from the optical analysis (k = 1.0) does not give the correct g value. The orbital reduction factor needed to fit the measured g value for $Np(BD_4)_4$ is less than that obtained from the ζ_{cry}/ζ_{FI} value of 0.93. The orbital reduction factor for $Np(BH_3CH_3)_4$ indicates a greater covalency for this molecule than in the unsubstituted $Np(BH_4)_4$ consistent with the magnetic results for $U(BH_4)_4$ and $U(BH_3CH_3)_4$.

Table 12. EPR results for $Np(BD_4)_4/Zr(BD_4)_4$ and $Np(BH_3CH_3)_4/Zr(BH_3CH_3)_4$ (Ref. 47)

k	g_{Γ_6} (calc)	g_{exp}
1.0	2.377	
0.885	1.896	1.896 [$Np(BD_4)_4/Zr(BD_4)_4$]
0.862	1.799	1.799 [$Np(BH_3CH_3)_4/Zr[BH_3CH_3)_4$]

6. Summary

The techniques and procedures utilized to obtain and interpret optical and magnetic data of f^n compounds have been described. Comparison of the Slater and spin-orbit parameters for free ions and the same ions in compounds allowed the determination of covalent effects. Measurements and data analyses on some $Cp_3Ln \cdot L$ compounds were described. The relative strengths of the crystal field in these compounds were approximately three times as large as found in the corresponding $Ln^{3+}/LaCl_3$ systems, although the Slater and spin-orbit parameters were similar.

ACKNOWLEDGEMENTS

I wish to thank Dr. W.T. Carnall for providing me with some of the information used in this presentation, Professor H.D. Amberger for allowing me to use some of his data and spectra, Mr. J. Brennan, Mr. P. Becker, and Dr. K. Rajnak for proofreading the manuscript and for their helpful comments, and B. Moriguchi and J. Bucher for their skill and patience in preparing this manuscript on a new word processor.

This work was supported by the Director, Office of Energy Research, Office of Basic Energy Sciences, Chemical Sciences Division of the U.S. Department of Energy under Contract No. DE-AC03-76SF00098.

REFERENCES

1. E.U. Cordon and G.H. Shortley, "The Theory of Atomic Spectra," Cambridge University Press, New York, 1935.
2. B.R. Judd, "Operator Techniques in Atomic Spectroscopy," McGraw-Hill, New York, 1963.
3. B.G. Wybourne, "Spectroscopic Properties of Rare Earths," Wiley, New York, 1965.
4. M. Tinkham, "Group Theory and Quantum Mechanics," McGraw-Hill, New York, 1964.
5. G.H. Dieke, "Spectra and Energy Levels of Rare Earth Ions in Crystals," Wiley, New York, 1968.
6. K. Rajnak and B. Wybourne, Phys. Rev. 132, 280 (1963).
7. B.R. Judd, Phys. Rev. 141, 4 (1966).
8. H.M. Crosswhite and H. Crosswhite, J. Opt. Soc. Am. B 1, 246 (1984).
9. W.C. Marten, R. Zalubas, and L. Hagen, "Atomic Energy Levels-The Rare-Earth Elements," NSRDS-NBS60, U.S. Government Printing Office, Washington, D.C., 1978.
10. C.H.H. Van Deurzen, K. Rajnak, and J.G. Conway, J. Opt. Soc. Am. B 1, 45 (1984).

11. J.F. Wyart, V. Kaufman, and J. Sugar, Physica Scripta 22, 389 (1980).
12. L. Brewer, J. Opt. Soc. Am. 61, 1666 (1971).
13. E. Loh, Phys. Rev 147, 332 (1966).
14. H.M. Crosswhite, H. Crosswhite, W.T. Carnall, and A.P. Paszek, J. Chem. Phys. 72, 5103 (1980).
15. D.S. McClure and Z. Kiss, J. Chem. Phys. 39, 3251 (1963).
16. E.K. Hulet in "Actinides in Perspective," N. Edelstein, Ed., Pergamon, Oxford, 1982, p. 453.
17. H.E. White, "Introduction to Atomic Spectra," McGraw-Hill, New York, 1934, p. 438.
18. N. Edelstein in "Organometallics of the f-Elements," T.J. Marks and R.D. Fischer, Eds., Reidel, Dordrecht, 1979, p. 37.
19. C.W. Nielson and G.F. Koster, "Specctroscopic Coefficients for the p^n, d^n, and f^n Configurations," MIT Press, Cambridge, MA., 1963.
20. J.H. Van Vleck, J. Phys. Chem. 41, 67 (1937).
21. S. Hufner, "Optical Spectra of Transparent Rare Earth Compounds," Academic Press, New York, 1978.
22. J.L. Prather, "Atomic Energy Levels in Crystals," NBS Monograph 19, Washington, D.C., 1961.
23. T. Hayhurst, G. Shalimoff, N. Edelstein, L.A. Boatner, and M.M. Abraham, J. Chem. Phys. 74, 5449 (1981).
24. T. Hayhurst, G. Shalimoff, J.G. Conway, N. Edelstein, L.A. Boatner, and M.M. Abraham, J. Chem. Phys. 76, 3960 (1982).
25. P. Delamoye, K. Rajnak, M.Genet, and N. Edelstein, Phys. Rev. B 28, 4923 (1983).
26. P.C. Becker, T. Hayhurst, G. Shalimoff, J.G. Conway, N. Edelstein, L.A. Boatner, and M.M. Abraham, J. Chem. Phys. 81, 2872 (1984).
27. G.F. Koster, J.O. Dimmock, R.G. Wheeler, and H. Statz, "Properties of the Thirty-Two Point Groups," MIT Press, Cambridge, MA., 1963.
28. R.G. Hayes and J.L. Thomas, Organometallic Chem. Rev. A 7, 1 (1971).

29. F. Calderazzo, R. Pappalardo, and S. Losi, J. Inorg. Nucl. Chem. 28, 987 (1966).
30. R. Pappalardo, Helv. Phys. Acta 38, 178 (1965).
31. R. Pappalardo and C.K. Jørgenson, J. Chem. Phys. 46, 632 (1967).
32. R. Pappalardo, J. Chem. Phys. 49, 1545 (1968).
33. R. Pappalardo, J. Molec. Spect. 29, 13 (1969).
34. H.-D. Amberger and W. Jahn, submitted to Spectrochimica Acta.
35. H.-D. Amberger, W. Jahn, and N. Edelstein, submitted to Spectrochimica A.
36. H.-D. Amberger, H. Schultze, and N. Edelstein, submitted to Spectrochimica A.
37. H.G. Brittain, J.H. Meadows, and W.J. Evans, Organometallics 2, 1661 (1983).
38. H.-D. Amberger and N. Edelstein, unpublished results, 1984.
39. J.H. Burns and W.H. Baldwin, J. Organomet. Chem. 120, 361 (1976).
40. R.D. Rogers, J.L. Atwood, E. Emad, D.J. Sikora, and M.D. Rausch, J. Organomet. Chem. 216, 383 (1981).
41. C. Gorller-Wallrand and J. Godemont, J. Chem. Phys. 66, 48 (1977).
42. C. Gorller-Wallrand, Y. Beyens, and J. Godemont, J. Chim. Phys. 76, 190 (1979).
43. F. Auzel and O.L. Malta, J. Phys. (Paris) 44, 201 (1983).
44. A.B.P. Lever, "Inorganic Electronic Spectroscopy," Elsevier, New York, 1968.
45. D.J. Newman, Austr. J. Phys. 30, 315 (1977).
46. M.V. Eremin and A.A. Kornienko, Opt. Spectrosc. (USSR) 53, 45 (1982).
47. K. Rajnak, R.H. Banks, E. Gamp, and N. Edelstein, J. Chem. Phys. 80, 5951 (1984).
48. K. Rajnak, E. Gamp, R. Shinomoto, and N. Edelstein, J. Chem. Phys. 80, 5924 (1984).

Appendix

Observed and calculated energies and g values for Tm^{3+} in $LuPO_4$.

Sym.	Energy (cm^{-1})		$g_{\|}$		Eig. Composition[a]			
	cal.	obs.	cal.	obs.	% largest	$(2S+1)L(J,J_z)$	% second	$(2S+1)L(J,J_z)$
Γ_1	0.0	0.0			71	$^3H(6,0)$	28	$^3H(6,\pm4)$
Γ_5	21.9	25.2	4.6	3.3	55	$^3H(6,-1)$	34	$^3H(6,-5)$
Γ_3	89.9	80.1			97	$^3H(6,\pm2)$	3	$^3H(6,\pm6)$
Γ_5	131.8	124.8	6.7	7.7	62	$^3H(6,-5)$	21	$^3H(6,-1)$
Γ_2	182.6				99	$^3H(6,\pm4)$		
Γ_1	248.2				71	$^3H(6,\pm4)$	28	$^3H(6,0)$
Γ_4	254.4				64	$^3H(6,\pm2)$	35	$^3H(6,\pm6)$
Γ_5	281.2		-4.3		73	$^3H(6,3)$	24	$^3H(6,-1)$
Γ_3	303.0				97	$^3H(6,\pm6)$	3	$^3H(6,\pm2)$
Γ_4	321.4				64	$^3H(6,\pm6)$	35	$^3H(6,\pm2)$
Γ_3	5587.0				62	$^3F(4,\pm2)$	30	$^1G(4,\pm2)$
Γ_5	5682.1	5674.0	-1.5		36	$^3F(4,-1)$	27	$^3F(4,3)$
Γ_1	5700.2				50	$^3F(4,\pm4)$	13	$^3F(4,0)$
Γ_2	5735.3				64	$^3F(4,\pm4)$	29	$^1G(4,\pm4)$
Γ_4	5769.3	5763.0			63	$^3F(4,\pm2)$	29	$^1G(4,\pm2)$
Γ_5	5844.4	5842.0	-3.0		37	$^3F(4,3)$	27	$^3F(4,-1)$
Γ_1	5856.7				51	$^3F(4,0)$	22	$^1G(4,0)$
Γ_2	8222.6	8227.0			62	$^3H(5,0)$	38	$^3H(5,\pm4)$
Γ_5	8257.7	8262.0	-0.2		67	$^3H(5,-1)$	30	$^3H(5,3)$
Γ_2	8384.7	8381.0			38	$^3H(5,0)$	62	$^3H(5,\pm4)$
Γ_5	8396.4	8395.0	-0.9		59	$^3H(5,3)$	23	$^3H(5,-5)$
Γ_3	8425.2				100	$^3H(5,\pm2)$		
Γ_5	8444.6	8441.0	7.3		74	$^3H(5,-5)$	16	$^3H(5,-1)$
Γ_1	12537.0	12530.8			55	$^3H(4,0)$	24	$^3F(4,0)$
Γ_5	12544.1	12535.2	-3.7	-3.7	45	$^3H(4,3)$	19	$^3F(4,3)$

$Tm^{3+}:LuPO_4$ (continued)

Sym.	Energy (cm^{-1}) cal.	obs.	$g_{\|}$ cal.	obs.	Eig. Composition[a] (2S+1)L(J,J_z) % largest		(2S+1)L(J,J_z) % second	
Γ_5	12672.6	12657.2	-0.1		44	3H(4,-1)	20	3F(4,-1)
Γ_3	12676.8				58	3H(4,±2)	28	3F(4,±2)
Γ_2	12704.7				59	3H(4,±4)	27	3F(4,±4)
Γ_1	12723.3				54	3H(4,±4)	24	3F(4,±4)
Γ_4	12782.6	12778.2			59	3H(4,±2)	27	3F(4,±2)
Γ_5	14404.6	14402.3	-4.3	-5.4	74	3F(3,3)	25	3F(3,-1)
Γ_5	14429.8	14435.3	0.0		74	3F(3,-1)	25	3F(3,3)
Γ_4	14438.4	14454.2			99	3F(3,±2)		
Γ_3	14452.2				99	3F(3,±2)		
Γ_2	14497.3				100	3F(3,0)		
Γ_4	14976.7	14964.0			75	3F(2,±2)	22	1D(2,±2)
Γ_5	15080.5	15087.8	1.5		76	3F(2,-1)	21	1D(2,-1)
Γ_1	15080.5				77	3F(2,0)	21	1D(2,0)
Γ_3	15083.8				77	3F(2,±2)	21	1D(2,±2)
Γ_3	20991.9	20983.0			57	1G(4,±2)	34	3H(4,±2)
Γ_5	21133.6		-0.9		37	1G(4,-1)	21	1G(4,3)
Γ_1	21178.9				21	1G(4,0)	37	1G(4,±4)
Γ_2	21257.5				57	1G(4,±4)	33	3H(4,±4)
Γ_4	21267.5	21278.3			57	1G(4,±2)	33	3H(4,±2)
Γ_5	21381.7	21394.1	-3.0		37	1G(4,3)	21	1G(4,-1)
Γ_1	21389.5				37	1G(4,0)	20	3H(4,0)
Γ_3	27755.7	27749.7			41	3P(2,±2)	40	1D(2,±2)
Γ_4	27793.6	27785.0			41	1D(2,±2)	39	3P(2,±2)
Γ_5	27818.8	27838.9	2.3		41	3P(2,-1)	41	1D(2,-1)
Γ_1	27837.6				41	1D(2,0)	40	3P(2,0)
Γ_4	34576.2	34579.0			97	1I(6,±2)	2	1I(6,±6)

$Tm^{3+}:LuPO_4$ (continued)

Sym.	Energy (cm^{-1}) cal.	obs.	$g_{\|}$ cal.	obs.	Eig. Composition[a] (2S+1)L(J,J_z) % largest		(2S+1)L(J,J_z) % second	
Γ_5	34595.4	34595.0	-0.9		57	1I(6,-1)	39	1I(6,3)
Γ_1	34613.4				65	1I(6,0)	33	1I(6,±4)
Γ_2	34834.3				99	1I(6,±4)		
Γ_3	34834.6				66	1I(6,±2)	33	1I(6,±6)
Γ_5	34846.4	34842.0	-0.2		52	1I(6,3)	24	1I(6,-5)
Γ_4	34911.9				97	1I(6,±6)	2	1I(6,±2)
Γ_3	34940.2				66	1I(6,±6)	33	1I(6,±2)
Γ_1	34951.7				33	1I(6,0)	66	1I(6,±4)
Γ_5	34974.0		7.1		71	1I(6,-5)	20	1I(6,-1)
Γ_1	35224.9	35238.0			93	3P(0,0)	6	1S(0,0)
Γ_2	36216.9				100	3P(1,0)		
Γ_5	36276.5	36266.0	3.0		100	3P(1,-1)		
Γ_4	37862.0				58	3P(2,±2)	38	1D(2,±2)
Γ_5	38049.4	38045.0	2.6		57	3P(2,-1)	38	1D(2,-1)
Γ_1	38049.5				58	3P(2,0)	38	1D(2,0)
Γ_3	38091.4				57	3P(2,±2)	39	1D(2,±2)
Γ_1	73579.9				94	1S(0,0)	6	3P(0,0)

[a]When the symbol ± appears in front of J_z the contributions from $+J_z$ and $-J_z$ are equal and have been summed. See reference 24 for a description of the eigenvectors of the Γ_i states.

TECHNICAL INFORMATION DEPARTMENT
LAWRENCE BERKELEY LABORATORY
UNIVERSITY OF CALIFORNIA
BERKELEY, CALIFORNIA 94720